

Journal of Mechanics of Materials and Structures

**THEREOTICAL SOLUTIONS OF ADHESIVE STRESSES
IN BONDED COMPOSITE BUTT JOINTS**

Gang Li

Volume 7, No. 4

April 2012

 **mathematical sciences publishers**

THEREOTICAL SOLUTIONS OF ADHESIVE STRESSES IN BONDED COMPOSITE BUTT JOINTS

GANG LI

In this paper, closed-form solutions for the adhesive stresses in bonded composite single-strap butt joints have been obtained. Two strategies were used for deriving the adhesive peel stress. The solutions are applicable to a butt joint made from different adherend and doubler laminates, as well as the unbalanced single-lap joints. In addition, three-dimensional finite element models of the unit-width composite joints were created for analyzing the adhesive stresses under a plane strain condition. A total of six joint conditions, three joint configurations and each with two layup sequences, were studied. Consistency in the peel stress predictions was obtained from the two theoretical strategies. Good agreement has been achieved between the theoretical and finite element results. The effects of the doubler thickness and laminate layup sequence on the adhesive stress variation can be displayed. The theoretical solution would provide a solid foundation for supporting the practical composite joint assessment.

A list of symbols can be found on page 345.

1. Introduction

With the recent advances in automated fiber placement equipment, composites can be effectively and extensively used in various aircraft structures. A recent example is the fuselage structure being fabricated for the Boeing 787, where large composite barrel sections are assembled. To this end, the composite joints used are critical. One possible joint option for these types of structures is the single-strap butt joint configuration. Typical attachments considered could be bonding, bolting, bonded-bolted joining, etc.

Bonded joints using adhesives with high moduli and strength would have much higher joint static strength than bolted joints [Li et al. 2012]. To improve the structural integrity, mechanical fasteners can be introduced using a hybrid (bonded-bolted) attachment approach [Kelly 2006; Li et al. 2012]. For the bonded single-strap butt joint configuration, high peak adhesive stresses exist at the bonded overlap edges, especially at the inner overlap edges [Hart-Smith 1985]. To evaluate the joint performance, the adhesive stress profiles are crucial and need to be fully understood first for further joint improvement. This is the subject of the current study.

The single-strap butt joint is actually fabricated by attaching two single-lap joints end-to-end, as shown in Figure 1. The same adhesive stress equilibrium equations exist between the single-strap and single-lap joints. Therefore, theoretical progress in the bonded single-lap joint can be applied to the single-strap butt joint. The elastic analysis of the bonded joints can be first traced back to [Volkersen 1938]. To date, elastic closed-form adhesive stress solution of the balanced single-lap joint has been well established [Goland

MSC2010: 00A05.

Keywords: adhesive stresses, closed-form solutions, composite single-strap butt joint, finite element analysis.

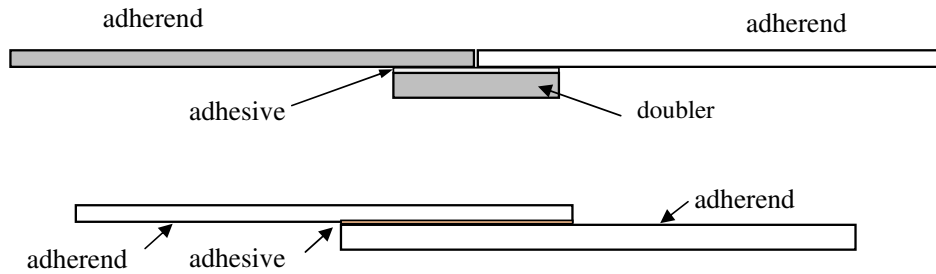


Figure 1. Schematic diagrams for a single-strap butt (top) and a single-lap joint (bottom).

and Reissner 1944; Hart-Smith 1973; Chen and Cheng 1983; Oplinger 1994; Li and Lee-Sullivan 2006a; Li and Lee-Sullivan 2006b]. When the two adherends have different geometries and/or mechanical properties, the single-lap joints are referred to as unbalanced. Due to the coupling relationship between the adhesive peel and shear stresses in the unbalance single-lap joint, the complexity of the analysis of this joint configuration is much higher than that of the balanced case. The corresponding closed-form adhesive stress solutions have not been provided by previous researchers [Hart-Smith 1973; Bigwood and Crocombe 1989; Cheng et al. 1991].

Coupling relationship between the adhesive shear and peel stresses is present in a general butt joint configuration with different doubler and adherends. Delale et al. [1981] reported their theoretical study on a bonded panel-to-substrate joint structure, a kind of butt joint configuration. The uncoupled seventh-order differential equation for adhesive shear stress was provided. They gave general expressions of the closed-form solutions for adhesive shear and peel stresses using complex terms with non-zero imaginary terms. The associated integral constants and the final solutions of the adhesive stresses were not further investigated. Bigwood and Crocombe [1989] obtained the uncoupled sixth-order differential equation for the adhesive peel stress. The final closed-form stress solutions were not fully provided.

To obtain the closed-form adhesive stress solutions using explicit expressions in bonded composite butt joints, the following theoretical preparations were made in [Li 2008; 2010; Li et al. 2011]:

- (1) This kind of closed-form stress solutions was obtained for the butt joint using isotropic materials.
- (2) The effective Young's modulus and bending stiffness were identified for laminate beam panels.
- (3) Expressions were provided for the four coefficients arising from the coupled adhesive stress differential equations in composite butt joint.
- (4) A theoretical strategy for exploring adhesive peel and shear stresses was presented.

Closed-form stress solutions were successfully obtained and are presented in the current paper. Two strategies were used to derive the adhesive peel stress solutions. To effectively demonstrate the theoretical solution, three-dimensional finite element models using twenty-node brick elements were created for analyzing the unit-width joints under a plane strain condition. A total of six joint conditions, three joint configurations with two layup sequences each, were studied. One joint configuration, case 1, was a special butt joint case made of identical laminates. The other two, cases 2 and 3, were general butt joints with different adherends and doubler in bending stiffness. For the sake of brevity, only the adhesive stress solutions and the associated comparisons are present. A quantitative study of the effect of various

factors on the adhesive stress magnitude can be carried out using the obtained solutions, which is not included in the paper. The theoretical solutions would make a sound basis for practical composite butt joint applications in the aerospace industry.

2. Theoretical formulation

Joint deformation and its loading condition. A typical configuration for a bonded composite single-strap butt joint is shown in Figure 2. The two adherends are made from identical laminates, which can be different from the doubler laminate. Due to load path eccentricity, secondary bending occurs when the joint is loaded in tension. Solutions of the joint deflection, elongation, bending moment, and strain at the overlap edge region were given in [Li et al. 2011]. For a thin adhesive layer, the equations relating the adhesive stress to the joint deformation are

$$\frac{\sigma_a}{E_a} = \frac{w_u - w_d}{\eta}, \quad \frac{\tau_a}{G_a} = \frac{u_u - u_d}{\eta}, \tag{1a}$$

where E_a and G_a are adhesive Young’s and shear moduli; η is the adhesive thickness, w_u and w_d are deflections in the upper adherend and doubler and u_u and u_d are displacements in the adherend at the adherend-adhesive interface and in the doubler at the adhesive-doubler interface.

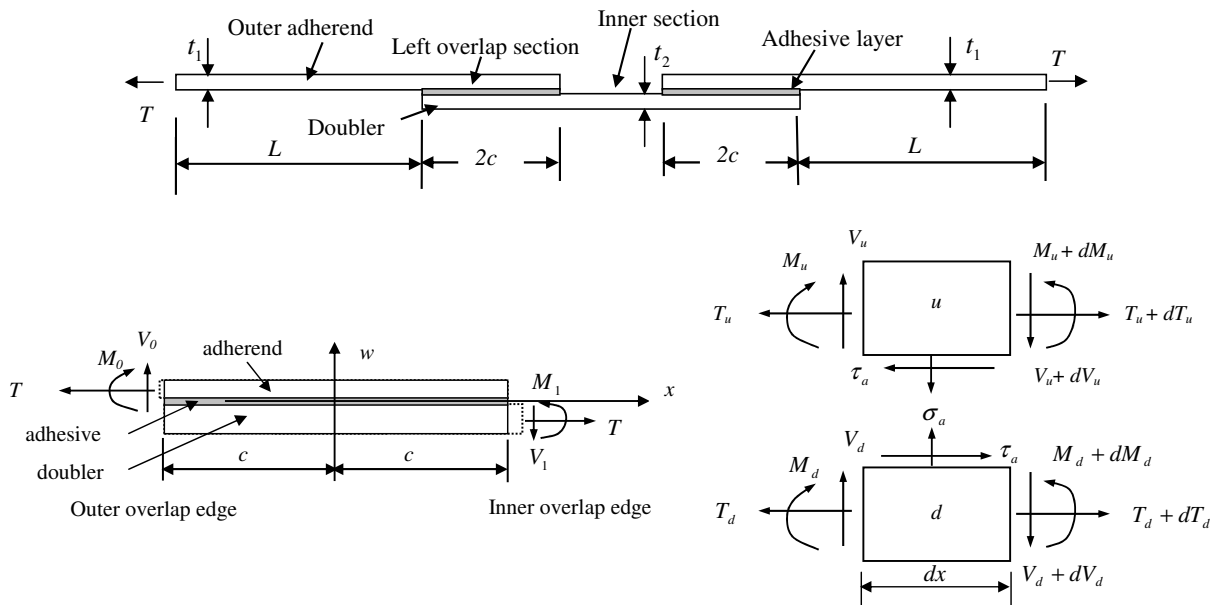


Figure 2. Top: a bonded composite butt joint in tension. Bottom left: forces at the overlap edges. Bottom right: the loading state in infinitesimal elements for upper adherend (denoted by u) and doubler (d) in the overlap section.

The axial strains of the adherend-adhesive and adhesive-doubler interfaces are

$$\begin{aligned}\epsilon_{x,\text{adh}} &= \frac{du_u}{dx} = \epsilon_{x,\text{adh}}^0 + \frac{1}{2}t_1\kappa_{x,\text{adh}} = k_{11,\text{adh}}T_u + k_{12,\text{adh}}M_u + \frac{1}{2}t_1\kappa_{x,\text{adh}} \\ &= k_{11,\text{adh}}T_u + k_{12,\text{adh}}M_u + \frac{1}{2}t_1(k_{12,\text{adh}}T_u + k_{22,\text{adh}}M_u),\end{aligned}\quad (1b)$$

$$\begin{aligned}\epsilon_{x,\text{doub}} &= \frac{du_d}{dx} = \epsilon_{x,\text{doub}}^0 - \frac{1}{2}t_2\kappa_{x,\text{doub}} = k_{11,\text{doub}}T_d + k_{12,\text{doub}}M_d - \frac{1}{2}t_2\kappa_{x,\text{doub}} \\ &= k_{11,\text{doub}}T_d + k_{12,\text{doub}}M_d - \frac{1}{2}t_2(k_{12,\text{doub}}T_d + k_{22,\text{doub}}M_d),\end{aligned}\quad (1c)$$

where the k_{ij} terms are compliances in the associated laminate in-plane constitutive equation [Li et al. 2011], as defined by (A.1a) in the Appendix.

Governing differential equations for adhesive stresses. The coupled adhesive stress differential equations for a single-strap butt joint are identical to those of a single-lap joint, except for the loading boundary conditions at the overlap edges. Through equilibrium analysis in the bonded overlap section, the adhesive stress equations can be derived (see [Cheng et al. 1991; Li 2008; 2010; Li et al. 2011]):

$$\frac{d^3\tau_a}{dx^3} + a_1\frac{d\tau_a}{dx} + a_2\sigma_a = 0, \quad \frac{d^4\sigma_a}{dx^4} + b_1\sigma_a + b_2\frac{d\tau_a}{dx} = 0, \quad (2a)$$

where a_1 , a_2 , b_1 , and b_2 , are four basic parameters to be determined prior to the exploration of the adhesive peel and shear stresses, σ_a and τ_a . The coupling parameters a_2 and b_2 vanish when dealing with identical materials having the same thickness for the adherends and doubler. The four parameters are determined in [Li et al. 2011] to be

$$\begin{aligned}a_1 &= -\frac{G_a}{\eta}(k_{11,\text{adh}} + k_{11,\text{doub}} + \frac{1}{2}t_1k_{12,\text{adh}} - \frac{1}{2}t_2k_{12,\text{doub}}) \\ &\quad - \frac{G_a}{\eta}\left(\frac{1}{2}(t_1 + \eta)(k_{12,\text{adh}} + \frac{1}{2}t_1k_{22,\text{adh}}) - \frac{1}{2}(t_2 + \eta)(k_{12,\text{doub}} - \frac{1}{2}t_2k_{22,\text{doub}})\right),\end{aligned}\quad (2b)$$

$$a_2 = \frac{G_a}{\eta}(k_{12,\text{adh}} + k_{12,\text{doub}} + \frac{1}{2}t_1k_{22,\text{adh}} - \frac{1}{2}t_2k_{22,\text{doub}}), \quad (2c)$$

$$b_1 = \frac{E_a}{\eta}(k_{22,\text{adh}} + k_{22,\text{doub}}), \quad (2d)$$

$$b_2 = -\frac{E_a}{\eta}\left(k_{12,\text{adh}} + k_{12,\text{doub}} + k_{22,\text{adh}}\frac{1}{2}(t_1 + \eta) - k_{22,\text{doub}}\frac{1}{2}(t_2 + \eta)\right), \quad (2e)$$

where the k_{ij} terms are presented in the Appendix.

3. Solutions for the adhesive stresses

Definitions of the butt joints in general and special cases. The general case refers to joints with different adherends and doubler in materials and/or thicknesses. The special case refers to joints with the coupling parameters $a_2 = b_2 = 0$. For this situation, the adhesive peel and shear stresses can be decoupled as in the balanced single-lap joints and it is easy to obtain the closed-form solutions [Bigwood and Crocombe 1989; Cheng et al. 1991; Hart-Smith 1973; Li and Lee-Sullivan 2006a; Li and Lee-Sullivan 2006b].

Efforts to explore the closed-form solutions are carried out for the general butt joint case in the following.

A special joint case: $a_2 = b_2 = 0$. The special joints are made from identical, symmetric and balanced laminates. In this case, the parameters are $k_{12} = 0$, $t_1 = t_2 = t$, and $k_{22,adh} = k_{22,doub} = k_{22}$. For thin adhesive layer, the other two parameters are

$$a_1 \approx -\frac{G_a}{\eta}(2k_{11} + \frac{t^2}{2}k_{22}) \quad \text{and} \quad b_1 = \frac{2E_a}{\eta}(k_{22}). \quad (3a)$$

The decoupled shear and peel stress equations would be

$$\frac{d^3\tau_a}{dx^3} + a_1\frac{d\tau_a}{dx} = 0, \quad \frac{d^4\sigma_a}{dx^4} + b_1\sigma_a = 0. \quad (3b)$$

Adhesive shear stress in the special joint case. The general solution for the adhesive shear stress is then

$$\tau_a = C_{0S} + C_{1S} \cosh(x\sqrt{-a_1}) + C_{2S} \sinh(x\sqrt{-a_1}). \quad (3c)$$

The expressions for the three constants C_{0S} , C_{1S} and C_{2S} , given in the Appendix, are determined using the following three boundary conditions:

$$\int_{-c}^c \tau_a dx = -T, \quad \left. \frac{d\tau_a}{dx} \right|_{x=-c} = \frac{G_a}{\eta}(k_{11}T + \frac{1}{2}tk_{22}M_0), \quad \left. \frac{d\tau_a}{dx} \right|_{x=c} = \frac{G_a}{\eta}(-k_{11}T + \frac{1}{2}tk_{22}M_1). \quad (3d)$$

The first boundary condition is the equilibrium relationship in the adherend between the applied tensile load and the integral of the resulting shear stress in the adhesive layer. The second and third boundary conditions relate the first derivative of shear stress to the loads at two overlap edges, which are obtained by combining the first derivative of the adhesive shear stress in (1a)₂ and the expressions of axial strains at the adherend-adhesive and adhesive-doubler interfaces in (1b) and (1c).

Adhesive peel stress in the special joint case. The general solution for the adhesive peel stress is

$$\begin{aligned} \sigma_a = & C_{3S} \cosh x(\sqrt[4]{b_1/4}) \cos x(\sqrt[4]{b_1/4}) + C_{4S} \sinh x(\sqrt[4]{b_1/4}) \cos x(\sqrt[4]{b_1/4}) \\ & + C_{5S} \cosh x(\sqrt[4]{b_1/4}) \sin x(\sqrt[4]{b_1/4}) + C_{6S} \sinh x(\sqrt[4]{b_1/4}) \sin x(\sqrt[4]{b_1/4}). \end{aligned} \quad (3e)$$

The four constants C_{3S}, \dots, C_{6S} , given in the Appendix, are determined using the boundary conditions

$$\left. \frac{d^2\sigma_a}{dx^2} \right|_{x=-c} = \frac{E_a}{\eta}k_{22}M_0, \quad \left. \frac{d^2\sigma_a}{dx^2} \right|_{x=c} = -\frac{E_a}{\eta}k_{22}M_1, \quad \left. \frac{d^3\sigma_a}{dx^3} \right|_{x=-c} = \frac{E_a}{\eta}k_{22}V_0, \quad \left. \frac{d^3\sigma_a}{dx^3} \right|_{x=c} = -\frac{E_a}{\eta}k_{22}V_1.$$

These four boundary conditions relate the derivatives of adhesive peel stress with the applied loads at the outer and inner overlap edges of the balanced butt joint.

The general joint case: $a_2 \neq 0$, $b_2 \neq 0$.

Adhesive shear stress in the general joint case. The uncoupled equation for the adhesive shear stress can be obtained by eliminating the peel stress in (2a)₁:

$$\frac{d^7\tau_a}{dx^7} + a_1\frac{d^5\tau_a}{dx^5} + b_1\frac{d^3\tau_a}{dx^3} + (a_1b_1 - a_2b_2)\frac{d\tau_a}{dx} = 0 \quad (4a)$$

The corresponding characteristic equation becomes (see [Derrick and Grossman 1987; Kreyszig 1993]):

$$\lambda(\lambda^6 + a_1\lambda^4 + b_1\lambda^2 + (a_1b_1 - a_2b_2)) = 0. \quad (4b)$$

The seven roots were previously obtained through complicated mathematical analyses in [Li 2010; Li et al. 2011]. The seven λ roots are given in the Appendix. Provided $\phi_1 = \gamma_1 - a_1/3 \geq 0$, the general solution for the adhesive shear stress can be established as

$$\begin{aligned} \tau_a = & C_0 + C_1 \cosh(x\sqrt{\gamma_1 - a_1/3}) + C_2 \sinh(x\sqrt{\gamma_1 - a_1/3}) \\ & + C_3 \cosh(x(|\phi|^{1/2} \cos \frac{\beta}{2})) \cos(x(|\phi|^{1/2} \sin \frac{\beta}{2})) + C_4 \sinh(x(|\phi|^{1/2} \cos \frac{\beta}{2})) \cos(x(|\phi|^{1/2} \sin \frac{\beta}{2})) \\ & + C_5 \cosh(x(|\phi|^{1/2} \cos \frac{\beta}{2})) \sin(x(|\phi|^{1/2} \sin \frac{\beta}{2})) + C_6 \sinh(x(|\phi|^{1/2} \cos \frac{\beta}{2})) \sin(x(|\phi|^{1/2} \sin \frac{\beta}{2})), \end{aligned} \quad (5a)$$

where the augment symbols ϕ and β have the same expression as in [Li 2010; Li et al. 2011] and are not spelled out here. The seven integral constants C_0, \dots, C_6 , given in the Appendix, are determined using the seven boundary conditions

$$\begin{aligned} \int_{-c}^c \tau_a dx &= -T, \\ \frac{d\tau_a}{dx} \Big|_{x=-c} &= \frac{G_a}{\eta} \left((k_{11,\text{adh}} + \frac{1}{2}t_1k_{12,\text{adh}})T + (k_{12,\text{adh}} + \frac{1}{2}t_1k_{22,\text{adh}})M_0 \right), \\ \frac{d\tau_a}{dx} \Big|_{x=c} &= \frac{G_a}{\eta} \left((-k_{11,\text{doub}} + \frac{1}{2}t_2k_{12,\text{doub}})T + (-k_{12,\text{doub}} + \frac{1}{2}t_2k_{22,\text{doub}})M_1 \right), \quad (5b) \\ \frac{d^2\tau_a}{dx^2} + a_1\tau_a \Big|_{x=-c} &= \frac{G_a}{\eta} (k_{12,\text{adh}} + \frac{1}{2}t_1k_{22,\text{adh}})V_0, \quad \frac{d^5\tau_a}{dx^5} + a_1\frac{d^3\tau_a}{dx^3} \Big|_{x=-c} = -a_2\frac{E_a}{\eta} (k_{12,\text{adh}}T + k_{22,\text{adh}}M_0), \\ \frac{d^2\tau_a}{dx^2} + a_1\tau_a \Big|_{x=c} &= \frac{G_a}{\eta} (\frac{1}{2}t_2k_{22,\text{doub}} - k_{12,\text{doub}})V_1, \quad \frac{d^5\tau_a}{dx^5} + a_1\frac{d^3\tau_a}{dx^3} \Big|_{x=c} = a_2\frac{E_a}{\eta} (k_{12,\text{doub}}T + k_{22,\text{doub}}M_1), \end{aligned}$$

where M_0 and V_0 are the bending moment and shear force at the outer overlap edge on the adherend, while M_1 and V_1 are the bending moment and shear force at the inner overlap edge on the doubler.

The first boundary condition in (5b) is obtained through the equilibrium relationship between joint adherend tensile load and the integral of the resulting shear stress in the adhesive layer. The other six boundary conditions relate different derivatives of adhesive shear stress at the outer and inner overlap edges with the applied loads at the same positions. Assuming continuity of strains at the adherend-adhesive and doubler-adhesive interfaces, as well as the continuity in the adhesive stress, the second and third boundary conditions at the two overlap edges are obtained by combining the first derivative of adhesive shear stress in (1a)₂ and the expressions of axial strains at the adherend-adhesive and adhesive-doubler interfaces in (1b) and (1c). Adhesive shear stress in (1a)₂ is differentiated twice and using the equilibrium equations of moment and tensile force to substitute for the fourth and fifth boundary conditions. To obtain the sixth and seventh boundary conditions for the uncoupled adhesive shear stress, two differentiations are applied to the adhesive stress equation in (2a)₁ with the aid of the peel stress expression in (1a)₁ and the moment-curvature relationship defined in the beam theory.

Current boundary conditions led to good agreement between the closed-form solutions of the proposed first strategy and FE results for the butt joints made of isotropic materials [Li 2010; Li et al. 2011], as well as the composite joints in the following section of the current paper.

First strategy: adhesive peel stress in the general joint case. Two strategies are presented to explore the closed-form adhesive peel stress solutions in bonded composite single-strap joints, provided the adhesive shear stress solution is known. The first is the one used in [Li 2010; Li et al. 2011], and good agreement was achieved between the theoretical and finite element results. The second was initially proposed in [Bigwood and Crocombe 1989].

The general solution of the adhesive peel stress can be explored using its fundamental equation, (2a)₂:

$$\frac{d^4\sigma_a}{dx^4} + b_1\sigma_a = -b_2\frac{d\tau_a}{dx}.$$

This nonhomogeneous equation can be investigated using variation of constants or Lagrange's method [Derrick and Grossman 1987; Kreyszig 1993]. The general solution is established by combining the solution of its homogeneous equation and any one particular solution of its nonhomogeneous equation. This strategy was successfully undertaken in [Li 2010; Li et al. 2011] and a detailed derivation of adhesive stresses in a bonded isotropic butt joint, where the general adhesive stress solutions were determined and good agreement was shown between closed-form solutions and finite element predictions.

The general solution of its homogeneous equation is

$$\begin{aligned}\sigma_{aH} = & C_{1H} \cosh x(\sqrt[4]{b_1/4}) \cos x(\sqrt[4]{b_1/4}) + C_{2H} \sinh x(\sqrt[4]{b_1/4}) \cos x(\sqrt[4]{b_1/4}) \\ & + C_{3H} \cosh x(\sqrt[4]{b_1/4}) \sin x(\sqrt[4]{b_1/4}) + C_{4H} \sinh x(\sqrt[4]{b_1/4}) \sin x(\sqrt[4]{b_1/4}).\end{aligned}\quad (6a)$$

One particular solution for its nonhomogeneous equation can be expressed in the form

$$\begin{aligned}\sigma_{ap} = & G_{1p}(x) \cosh x(\sqrt[4]{b_1/4}) \cos x(\sqrt[4]{b_1/4}) + G_{2p}(x) \sinh x(\sqrt[4]{b_1/4}) \cos x(\sqrt[4]{b_1/4}) \\ & + G_{3p}(x) \cosh x(\sqrt[4]{b_1/4}) \sin x(\sqrt[4]{b_1/4}) + G_{4p}(x) \sinh x(\sqrt[4]{b_1/4}) \sin x(\sqrt[4]{b_1/4}),\end{aligned}\quad (6b)$$

where the functions G_{1p}, \dots, G_{4p} are determined using the following simultaneous equations [Derrick and Grossman 1987; Kreyszig 1993], where we have set $Q = \sqrt[4]{b_1/4}$:

$$\begin{aligned}& G'_{1p}(x) \cosh x Q \cos x Q + G'_{2p}(x) \sinh x Q \cos x Q \\ & + G'_{3p}(x) \cosh x Q \sin x Q + G'_{4p}(x) \sinh x Q \sin x Q = 0, \\ & G'_{1p}(x) \frac{d}{dx} (\cosh x Q \cos x Q) + G'_{2p}(x) \frac{d}{dx} (\sinh x Q \cos x Q) \\ & + G'_{3p}(x) \frac{d}{dx} (\cosh x Q \sin x Q) + G'_{4p}(x) \frac{d}{dx} (\sinh x Q \sin x Q) = 0, \\ & G'_{1p}(x) \frac{d^2}{dx^2} (\cosh x Q \cos x Q) + G'_{2p}(x) \frac{d^2}{dx^2} (\sinh x Q \cos x Q) \\ & + G'_{3p}(x) \frac{d^2}{dx^2} (\cosh x Q \sin x Q) + G'_{4p}(x) \frac{d^2}{dx^2} (\sinh x Q \sin x Q) = 0, \\ & G'_{1p}(x) \frac{d^3}{dx^3} (\cosh x Q \cos x Q) + G'_{2p}(x) \frac{d^3}{dx^3} (\sinh x Q \cos x Q) \\ & + G'_{3p}(x) \frac{d^3}{dx^3} (\cosh x Q \sin x Q) + G'_{4p}(x) \frac{d^3}{dx^3} (\sinh x Q \sin x Q) = -b_2 \frac{d\tau_a}{dx}.\end{aligned}\quad (6c)$$

The expressions for $G_{1p}(x), \dots, G_{4p}(x)$ are very lengthy and can be found in [Li 2010], and thus are not included here. The solution for the adhesive peel stress in the general butt joint case is given by (again with $Q = \sqrt[4]{b_1/4}$)

$$\begin{aligned}\sigma_a &= \sigma_{aH} + \sigma_{ap} \\ &= C_{1H} \cosh x Q \cos x Q + C_{2H} \sinh x Q \cos x Q \\ &\quad + C_{3H} \cosh x Q \sin x Q + C_{4H} \sinh x Q \sin x Q \\ &\quad + G_{1p}(x) \cosh x Q \cos x Q + G_{2p}(x) \sinh x Q \cos x Q \\ &\quad + G_{3p}(x) \cosh x Q \sin x Q + G_{4p}(x) \sinh x Q \sin x Q.\end{aligned}\tag{6d}$$

The expressions for the four constants C_{1H}, \dots, C_{4H} , given in the Appendix, are determined using the boundary conditions

$$\begin{aligned}\frac{d^2\sigma_a}{dx^2}\Big|_{x=-c} &= \frac{E_a}{\eta}(k_{12,\text{adh}}T + k_{22,\text{adh}}M_0), & \frac{d^3\sigma_a}{dx^3} + b_2\tau_a\Big|_{x=-c} &= \frac{E_a}{\eta}k_{22,\text{adh}}V_0, \\ \frac{d^2\sigma_a}{dx^2}\Big|_{x=c} &= -\frac{E_a}{\eta}(k_{12,\text{doub}}T + k_{22,\text{doub}}M_1), & \frac{d^3\sigma_a}{dx^3} + b_2\tau_a\Big|_{x=c} &= -\frac{E_a}{\eta}k_{22,\text{doub}}V_1.\end{aligned}\tag{6e}$$

The above four boundary conditions relate the derivatives of adhesive peel stress with the applied loads at the outer and inner overlap edges. Two differentiations are conducted to the peel stress expression in (1a)₁ with the aid of the moment-curvature relationship to obtain the first two boundary conditions. One more differentiation is applied to the second derivative of the peel stress expression in (1a)₁ with the aid of moment equilibrium relationship to obtain the third and fourth boundary conditions.

Second strategy: adhesive peel stress in the general joint case. As mentioned before, this strategy was initially suggested by Bigwood and Crocombe in 1989. They did not present the associated boundary conditions for exploring the peel stress. To assess the possibility and difficulty in using this strategy, further adhesive stress exploration is conducted in the following.

The uncoupled sixth-order differential equation [Bigwood and Crocombe 1989] for adhesive peel stress can be derived by eliminating adhesive shear stress in (2a)₂ as

$$\frac{d^6\sigma_a}{dx^6} + a_1\frac{d^4\sigma_a}{dx^4} + b_1\frac{d^2\sigma_a}{dx^2} + (a_1b_1 - a_2b_2)\sigma_a = 0.\tag{7a}$$

The corresponding characteristic equation becomes

$$\lambda^6 + a_1\lambda^4 + b_1\lambda^2 + (a_1b_1 - a_2b_2) = 0.\tag{7b}$$

Note from the two uncoupled adhesive stress differential equations in (4a) and (7a), that their characteristic equations would have up to six common roots, λ_i ($i = 1$ to 6). One more characteristic root of $\lambda = 0$ exists for the adhesive shear stress.

The general solution for the adhesive peel stress can be established as:

$$\begin{aligned} \sigma_a = & C_{p1} \cosh\left(x\sqrt{\gamma_1 - a_1/3}\right) + C_{p2} \sinh\left(x\sqrt{\gamma_1 - a_1/3}\right) \\ & + C_{p3} \cosh\left(x(|\phi|^{1/2} \cos \frac{\beta}{2})\right) \cos\left(x(|\phi|^{1/2} \sin \frac{\beta}{2})\right) + C_{p4} \sinh\left(x(|\phi|^{1/2} \cos \frac{\beta}{2})\right) \cos\left(x(|\phi|^{1/2} \sin \frac{\beta}{2})\right) \\ & + C_{p5} \cosh\left(x(|\phi|^{1/2} \cos \frac{\beta}{2})\right) \sin\left(x(|\phi|^{1/2} \sin \frac{\beta}{2})\right) + C_{p6} \sinh\left(x(|\phi|^{1/2} \cos \frac{\beta}{2})\right) \sin\left(x(|\phi|^{1/2} \sin \frac{\beta}{2})\right). \end{aligned} \quad (7c)$$

The six integral constants C_{p1}, \dots, C_{p6} in the general peel stress solution expression may be determined using the following boundary conditions:

$$\begin{aligned} \int_{-c}^c \sigma_a dx &= V_u|_{x=-c} - V_u|_{x=c} = V_0, & \int_{-c}^c \sigma_a x dx &= -(V_0 c + M_0), \\ \frac{d^2 \sigma_a}{dx^2} \Big|_{x=-c} &= \frac{E_a}{\eta} (k_{12,\text{adh}} T + k_{22,\text{adh}} M_0), & \frac{d^3 \sigma_a}{dx^3} + b_2 \tau_a \Big|_{x=-c} &= \frac{E_a}{\eta} k_{22,\text{adh}} V_0, \\ \frac{d^2 \sigma_a}{dx^2} \Big|_{x=c} &= -\frac{E_a}{\eta} (k_{12,\text{doub}} T + k_{22,\text{doub}} M_1), & \frac{d^3 \sigma_a}{dx^3} + b_2 \tau_a \Big|_{x=c} &= -\frac{E_a}{\eta} k_{22,\text{doub}} V_1. \end{aligned} \quad (7d)$$

Similarly to the explanations of the boundary conditions (5b), the boundary conditions (7d) reflect the joint equilibrium state and internal relationship between the adhesive stresses and the associated laminate moment-curvature at different differentiation levels. The derived six integral constants are given in the Appendix. It can be seen from the derivations that the second strategy would avoid the complex derivations and long expressions required for determining the adhesive peel stress used in the first strategy.

Consistency of the adhesive stresses from the general to special joint cases. The derivations in the closed-form stress solutions were carried out based on their fundamental equations, thus, when the general case approaches the special butt joint case, both the adhesive peel and shear stresses will converge to their corresponding adhesive stresses in the special joint case, which have been validated elsewhere [Li 2010].

Consistency of the adhesive peel stresses between the two solution strategies in general joint case. For clarity and simplicity, numerical examples in Section 4 will be used to demonstrate the consistency.

4. Numerical examples and discussion

A total of six joint conditions were studied: three joint configurations and each with two layup sequences. Each of the selected joints have two identical 50 mm long unbonded outer adherends, a 101.6 mm long doubler including a 0.5 mm long inner section, and two identical 50.55 mm long adhesive layers of 0.17 mm in thickness. A 100 MPa remote tensile stress was applied to the joint adherend.

The 16-ply laminates were used for all the joint adherends. The only difference was the doubler laminates in the three joint configurations. The case 1 joint had identical 16-ply laminates for both the adherend and doubler, which makes it the special joint without a coupling effect between the adhesive peel and shear stresses. The doublers of the case 2 joint were made from 24-ply laminates, and the case 3 joint doublers were made from 32-ply laminates. The two layup sequences were $[45/-45/0/90]_{\text{ns}}$ and $[0/90/45/-45]_{\text{ns}}$ referred to as S1 and S2, respectively. The same layup sequence was used in each joint

laminates. For instance, C1S1 refers the case 1 joint made from the 16-ply $[45/-45/0/90]_{2s}$ laminates; and C2S2 refers the case 2 joint made from the 16-ply $[0/90/45/-45]_{2s}$ laminate adherend and 24-ply $[0/90/45/-45]_{3s}$ laminate doubler, etc. The laminates were generated using 0.14 mm thick carbon fiber laminae, and the lamina material properties were: $E_{11} = 145$ GPa, $E_{22} = 8.9$ GPa, $\nu_{12} = 0.31$, and $G_{12} = 4.5$ GPa based on our tests.

Determination of the adhesive stresses using the closed-form solutions. The first step is to determine the bending moments and shear forces at the bonded overlap edges as explained in [Li et al. 2011]. Then, according to the laminate layup condition and material properties, the four coefficients, a_1 , a_2 , b_1 , and b_2 from (2b)–(2e) are calculated. Finally, the adhesive stresses are determined using the solutions given in Section 3.

Finite element modeling. To properly set up the lamina orientation in each ply, three-dimensional finite element (FE) models with unit width (1 mm in the y -direction) were generated using MSC.Patran and MSC.Marc version 2010r1. Geometrically nonlinear behavior in the joint deformation under a two-dimensional plane strain condition was analyzed by applying the zero displacement condition, $U_y = 0$, at the two joint side edges over the entire joint length (x -direction). The joint width was in the y -axis direction, and thickness was in the z -direction. As shown in Figure 3, a fine mesh was applied to the

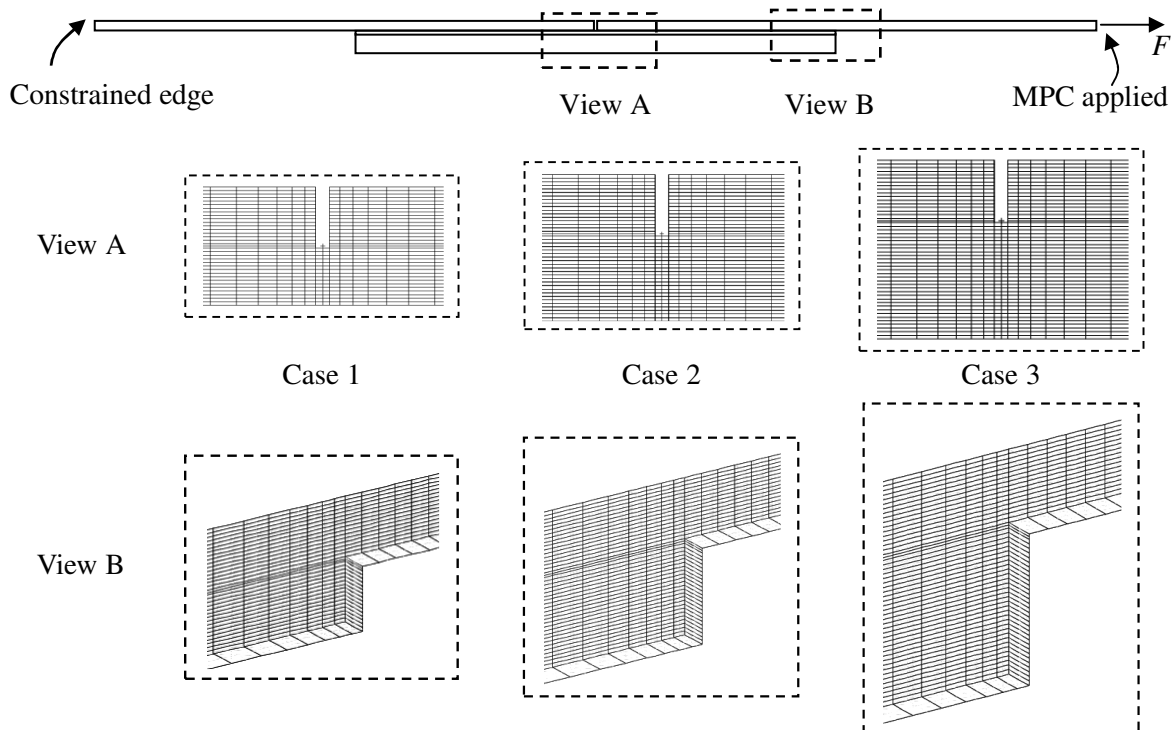


Figure 3. Schematic diagrams for the two simulated butt joints with a 0.5 mm inner gap section for both adherends and adhesive. Case 1: a joint made of identical 16-ply laminates. Case 2: a joint with 16-ply adherend and 24-ply doubler laminates. Case 3: a joint with 16-ply adherend and 32-ply doubler laminates.

overlap edge areas. Two elements were used through the adhesive thickness, while one element was used along the joint unit width as well as in each lamina in the thickness direction. A total of 2,404 twenty-node hexahedron brick elements with 17,561 nodes were created for the special case 1 joint. A total of 2,820 twenty-node hexahedron brick elements with 20,513 nodes were generated for the case 2 joint with the 24-ply doubler. A total of 3,236 twenty-node hexahedron brick elements with 23,465 nodes were generated for the case 3 joint with the 32-ply doubler. The convergence of the adhesive stress value was obtained using the current meshes in the FE models. The left edge was clamped without any displacement in both the horizontal and vertical directions, while the right adherend far end edge was uniformly loaded with a tensile stress of 100 MPa. Multi-point-constrain (MPC) conditions were applied to the right edge nodes ensuring the same displacement during the tensile loading stage. FE analysis results for each pair of nodes, located at the $[x, 0, z]$ and $[x, 1, z]$ positions on the two width side surfaces, were almost identical.

Comparison of the adhesive stresses between the closed-form solutions and FE results. Five nodes were used through the thickness of the adhesive layer. Adhesive stresses at the upper element mid-node (near adherend), adhesive centerline, and lower elements mid-node (near doubler) were extracted and analyzed.

Comparison of the adhesive peel stresses. Variations in the adhesive peel stresses obtained from closed-form solutions and finite element results are presented in Figures 4 to 9 for the three joint cases with two layups. For clarity, close views of the peak stress profiles at the inner bonded overlap edges are plotted. Good correlations were obtained between the theoretical and FE results for all the cases. The following details can be observed:

- (1) high stresses are present in the vicinity of the overlap edges, the highest being at the inner overlap edge position;

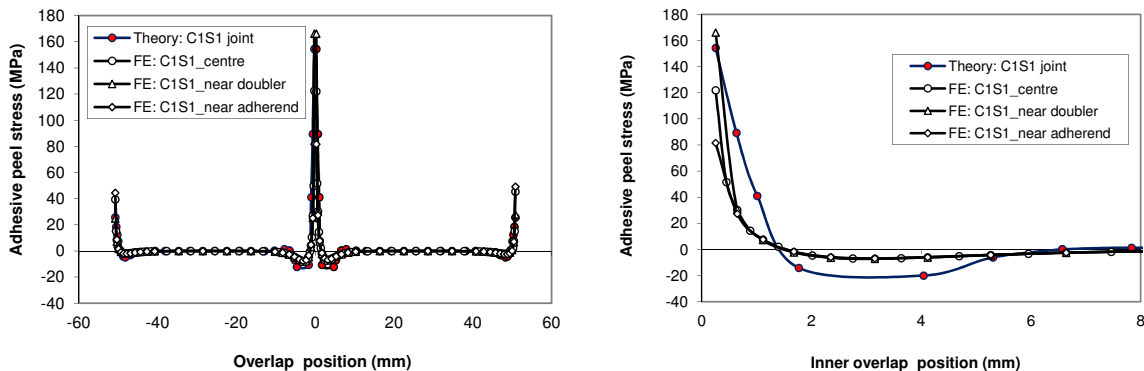


Figure 4. Comparison of the adhesive peel stresses obtained from closed-form solutions and FE results for a special butt C1S1 joint with the identical 16-ply laminates in $[45/-45/0/90]_{2s}$ layup condition. Left: adhesive peel stress profile through the bonded overlap. Right: Peak adhesive peel stress at the inner overlap edge region Here FE: C1S1_near doubler refers to the path along the mid-nodes of the adhesive layer elements adjacent to the doubler. Similar labels apply to the remaining figures.

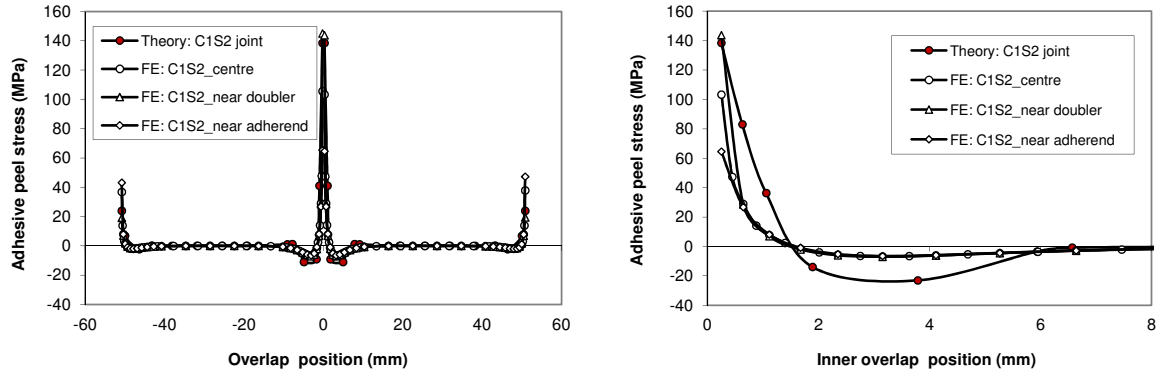


Figure 5. Comparison of the adhesive peel stresses obtained from closed-form solutions and FE results for a special butt C1S2 joint with the identical 16-ply laminates in $[0/90/45/-45]_{2s}$ layup condition.

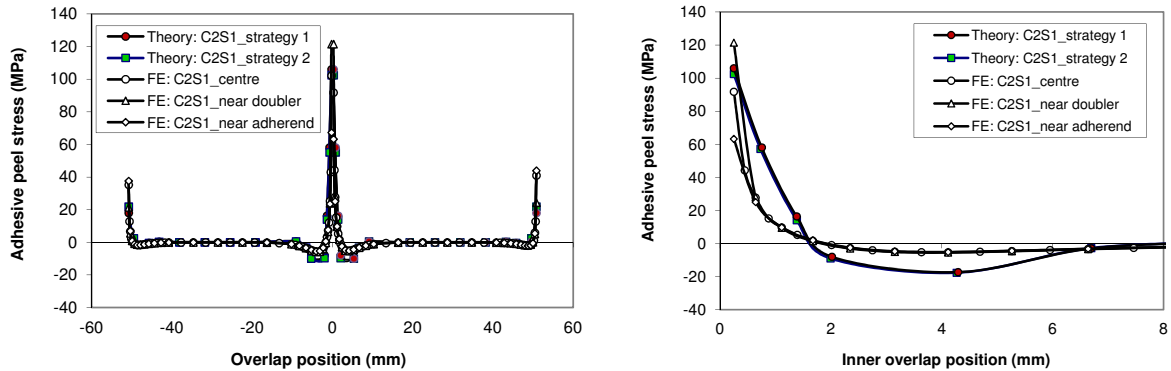


Figure 6. Comparison of the adhesive peel stresses obtained from closed-form solutions and FE results for a special butt C2S1 joint with the 16-ply adherend in $[45/-45/0/90]_{2s}$ layup and 24-ply doubler in $[45/-45/0/90]_{3s}$ layup condition.

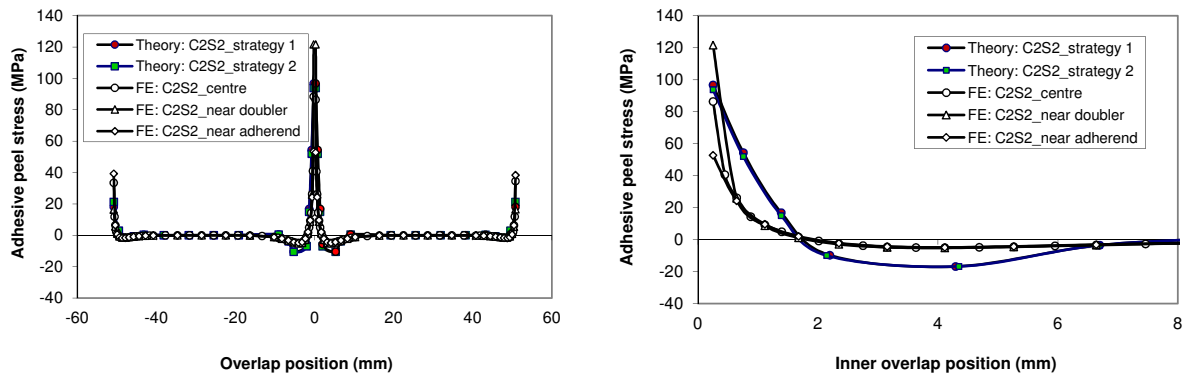


Figure 7. Comparison of the adhesive peel stresses obtained from closed-form solutions and FE results for a special butt C2S2 joint with the 16-ply adherend in $[0/90/45/-45]_{2s}$ layup and 24-ply doubler in $[0/90/45/-45]_{3s}$ layup condition.

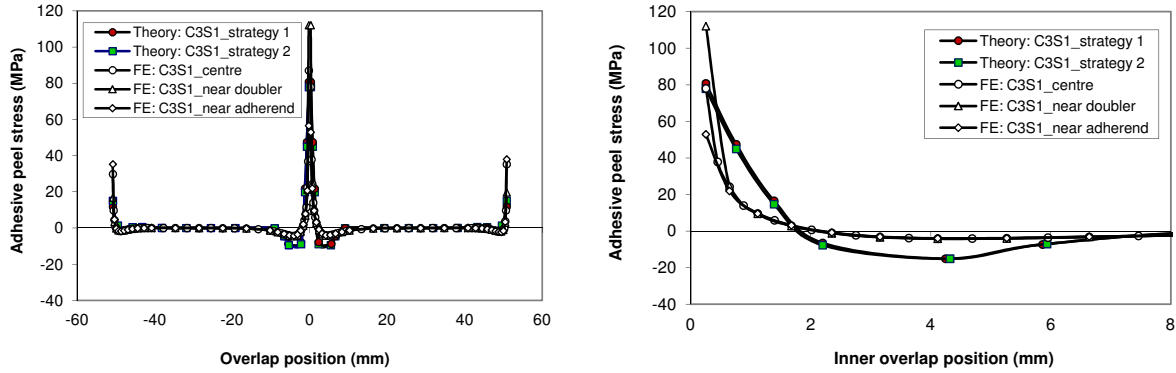


Figure 8. Comparison of the adhesive peel stresses obtained from closed-form solutions and FE results for a special butt C3S1 joint with the 16-ply adherend in $[45/-45/0/90]_{2s}$ layup and 32-ply doubler in $[45/-45/0/90]_{4s}$ layup condition.

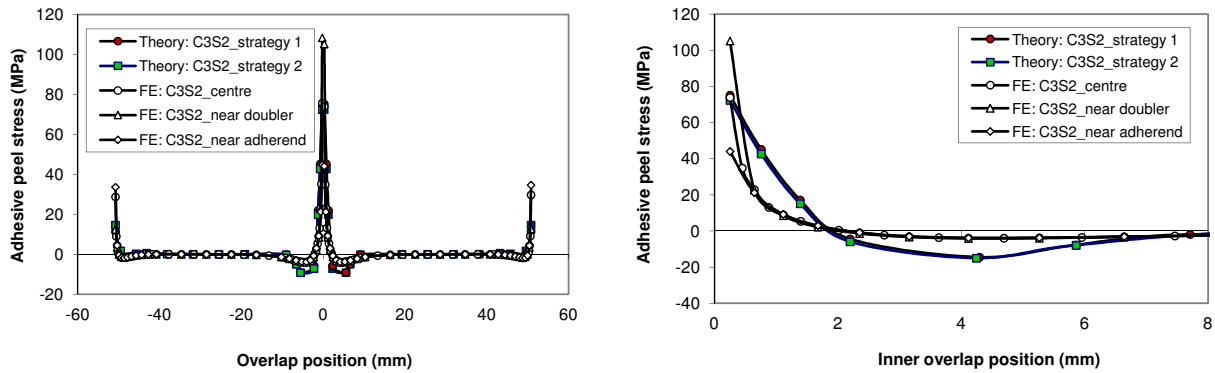


Figure 9. Comparison of the adhesive peel stresses obtained from closed-form solutions and FE results for a special butt C3S2 joint with the 16-ply adherend in $[0/90/45/-45]_{2s}$ layup and 32-ply doubler in $[0/90/45/-45]_{4s}$ layup condition.

- (2) the stress magnitudes are lower using the thicker doubler, as well as the S2 layup condition;
- (3) consistency in the adhesive peel stress magnitude obtained from the two theoretical strategies is demonstrated;
- (4) the theoretical results are approximately the same as the FE results, except at the edge positions; and
- (5) at the overlap edge position, the peel stress singularity can be obtained from both the theoretical and FE results with correlated peak stresses.

Comparison of the adhesive shear stresses. Figures 10 to 15 show the adhesive shear stress profiles for the six joint conditions. Both theoretical and FE results show that both the peel and shear stress magnitudes are affected by the doubler thickness and laminate layup condition. The direct reason could be the effective bending stiffness value. The S2 layup laminates have a higher bending stiffness than

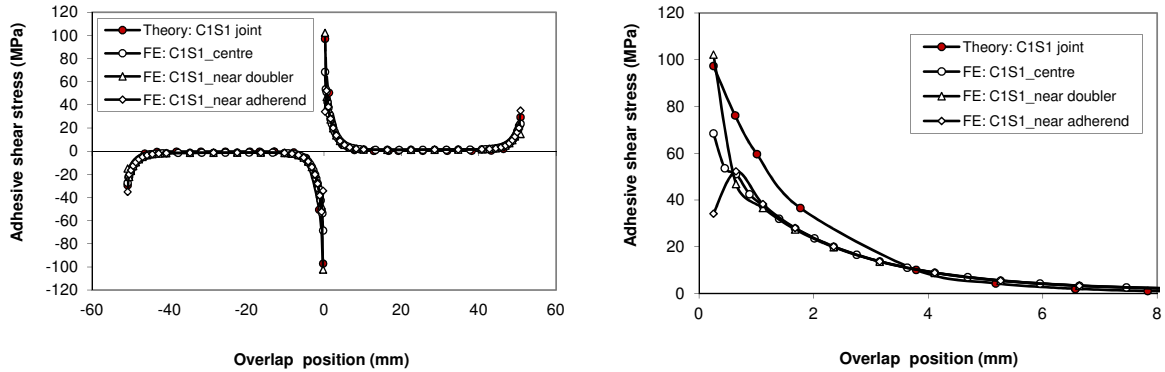


Figure 10. Comparison of the adhesive shear stresses obtained from closed-form solutions and FE results for a special butt C1S1 joint with the identical 16-ply laminates in $[45/-45/0/90]_{2s}$ layup condition.

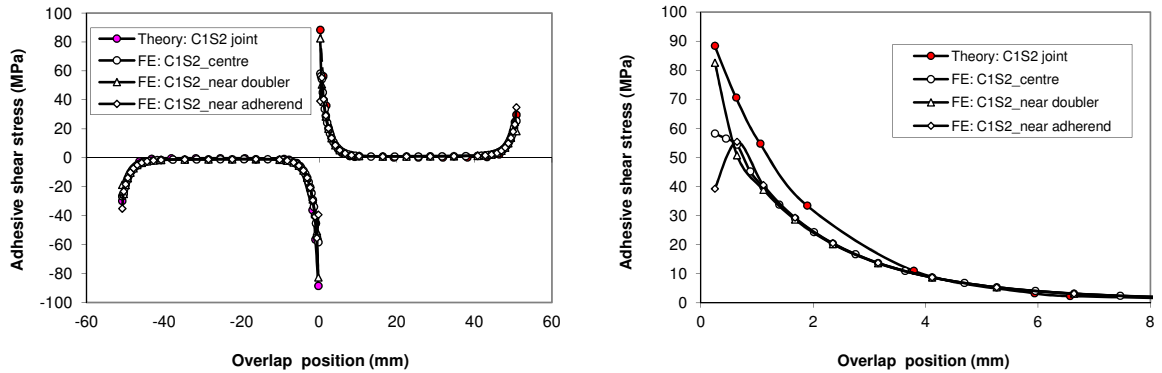


Figure 11. Comparison of the adhesive shear stresses obtained from closed-form solutions and FE results for a special butt C1S2 joint with the identical 16-ply laminates in $[0/90/45/-45]_{2s}$ layup condition.

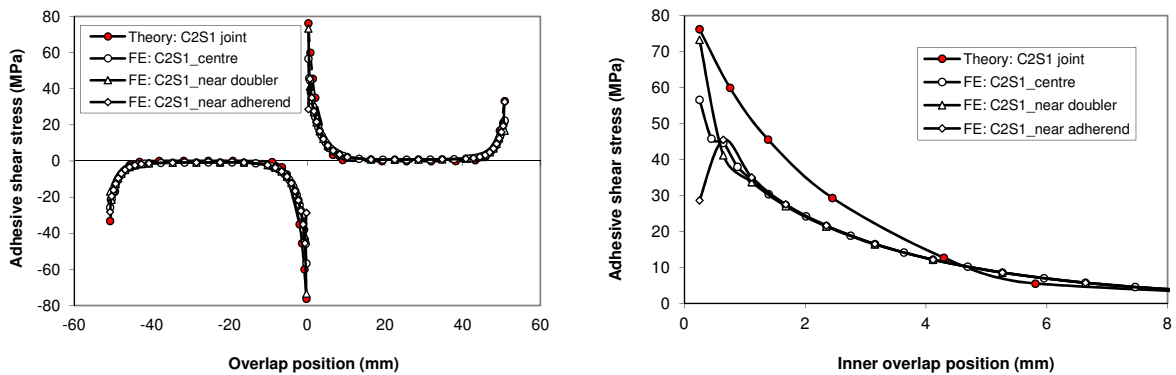


Figure 12. Comparison of the adhesive shear stresses obtained from closed-form solutions and FE results for a special butt C2S1 joint with the 16-ply adherend in $[45/-45/0/90]_{2s}$ layup and 24-ply doubler in $[45/-45/0/90]_{3s}$ layup condition.

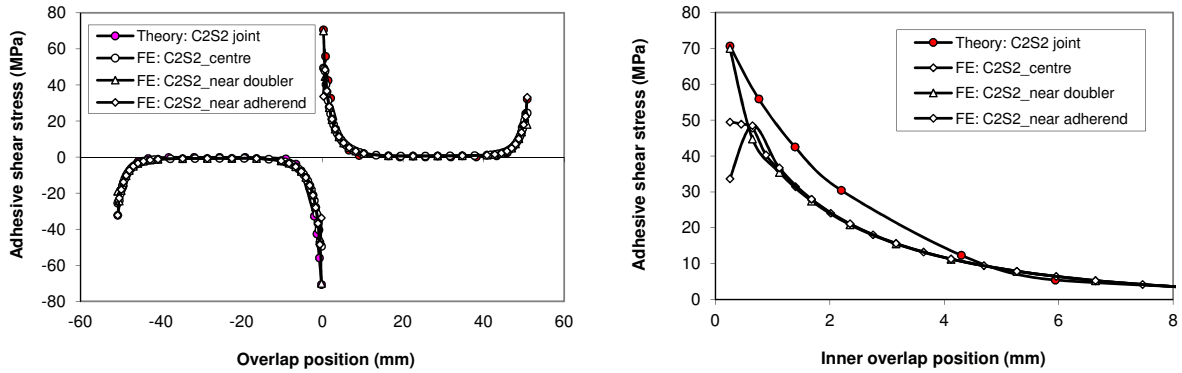


Figure 13. Comparison of the adhesive shear stresses obtained from closed-form solutions and FE results for a special butt C2S2 joint with the 16-ply adherend in $[0/90/45/-45]_{2s}$ layup and 24-ply doubler in $[0/90/45/-45]_{3s}$ layup condition.

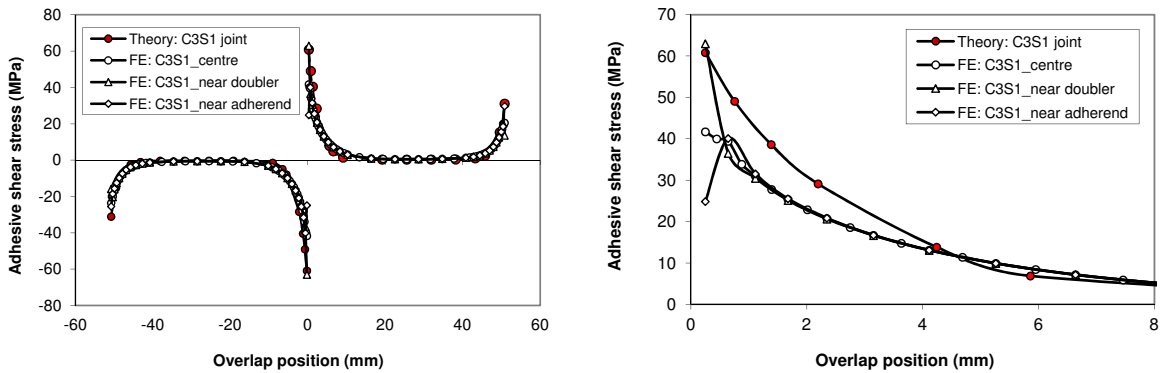


Figure 14. Comparison of the adhesive shear stresses obtained from closed-form solutions and FE results for a special butt C3S1 joint with the 16-ply adherend in $[45/-45/0/90]_{2s}$ layup and 32-ply doubler in $[45/-45/0/90]_{4s}$ layup condition.

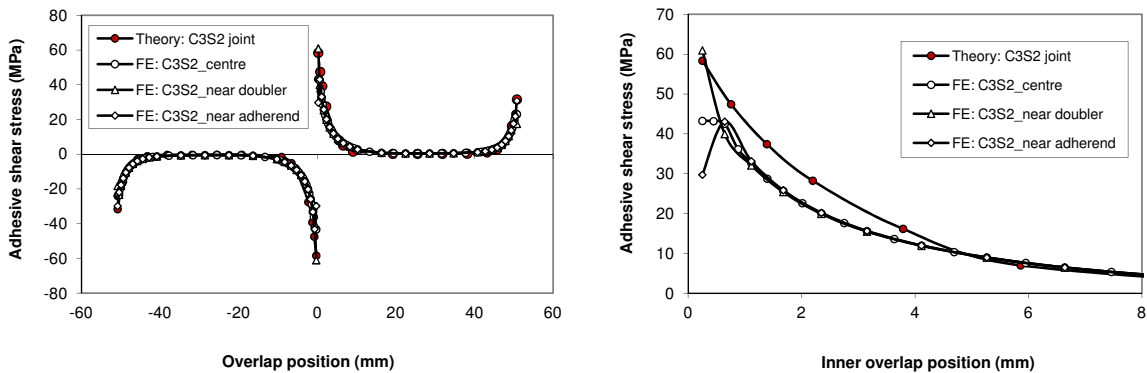


Figure 15. Comparison of the adhesive shear stresses obtained from closed-form solutions and FE results for a special butt C3S2 joint with the 16-ply adherend in $[0/90/45/-45]_{2s}$ layup and 32-ply doubler in $[0/90/45/-45]_{4s}$ layup condition.

the S1 laminates. Small bending deformations would be found in the joint using stiff laminates, and the resulting adhesive stresses magnitude should be small. Due to the shear stress free condition at the two inner adherend edges, the FE results for the adhesive shear stresses at the upper nodes near to the adhesive-adherend interface dropped at the edge positions, as shown in the right-hand portions of Figures 10 through 15. This drop cannot be obtained from the theoretical solutions due to the approximations used in (1a). A study of the correlation between the stress drop and the associated bending stiffness and/or doubler thickness could be carried out using the theoretical solutions, but is not covered in this paper.

The comparisons above clearly show that the closed-form stress solutions are reliable and accurate. The obtained results demonstrate that the current used boundary conditions are adequate. The closed-form stress solutions could be used to analyze the Mode I and Mode II strain energy release rate for cohesive crack propagation behavior or associated delamination in a generic situation of butt joints using the approach as in [Hu 1995; Li et al. 1999]. The adhesive stress profile clearly shows the high stressed area where further appropriate reinforcement work should be made to improve the joint structural integrity.

Factors affecting the adhesive stress magnitude. Typical factors affecting the adhesive stress include the thicknesses in the adherend, doubler, and adhesive, the inner doubler section length (a kind of cohesive crack length at the bonded butt joint mid-position area), the adhesive modulus, the laminate layup condition, etc. The impact of these factors could be investigated using the closed-form solutions, but this is not pursued in this report. To avoid tedious calculations in the adhesive peel stress, strategy 2 is recommended, since both strategies give almost identical peel stress results.

5. Conclusions

- (1) Closed-form adhesive stress solutions were obtained for the bonded composite single-strap butt joint. Strategy 2 would lead to a relative concise peel stress expression, as compared to the strategy 1. Generally, the integration constants in the closed-form adhesive stress solutions are quite long and complex, which is acceptable for such a complicated analysis of high order differential equations. The theoretical solution can be applied to the unbalanced composite single-lap joints, because the single-strap butt joint actually consists of two unbalanced single-lap joints. The complete theoretical solution can be the solid base for further development of simplified stress solutions for better practical applications of composite joint in the near future.
- (2) A total of six joint conditions: three joint configurations, each having two different layup sequences in laminates, were studied theoretically and numerically for demonstrating the theoretical correctness. Three-dimensional finite element models using twenty-node brick elements were created for the unit-width joints deformation analysis under plane strain condition.
- (3) Consistency in the predicted adhesive peel stresses were demonstrated using the two theoretical strategies; the small difference observed could be attributed to numerical error in the lengthy, complex, and sensitive terms in the closed-form solutions.
- (4) Good agreement was obtained in all the associated stress comparisons obtained from the theoretical and numerical results. High peak stress exists at the bonded overlap edges, with higher magnitude at the inner overlap edge.

- (5) Effects of doubler bending stiffness (e.g., thickness) and laminate layup sequence on the adhesive stress magnitude were revealed by both theoretical and numerical results. The thicker doubler led to the smaller peak stress magnitudes. Similarly, two used layup sequences, which had different laminate bending stiffness, also had different adhesive stress magnitudes. For instance, the bending stiffness of the S1 [45/−45/0/90]_{ns} laminates would be approximately 80% of the S2 [0/90/45/−45]_{ns} laminates, and the corresponding stress magnitudes for both peel and shear stresses are smaller in the S1 joints than the S2 joints, at a lesser degree. A practical evaluation of the adhesive stress profile under the influence of each joint component can be easily carried out using the obtained closed-form solutions, with the aid of an Excel spreadsheet tool.
- (6) The closed-form solutions would provide the insightful assessment to identify the proper hole positions for introducing extra fasteners to fabricate a strong hybrid attached, bonded-bolted, composite joint. In addition, extra strengthening should be applied to the geometrical transition areas, especially the inner overlap edge region to ensure structural integrity.

Acknowledgements

The full support from the Institute for Aerospace Research (IAR) is acknowledged and greatly appreciated. Many thanks to those people who have, in one way or another, contributed to this work.

Appendix: Expressions for relevant parameters in adhesive stresses

Effective parameters in laminated composite beam analysis [Li et al. 2011]. For the classic Euler–Bernoulli beam with no transverse loads, the in-plane laminate constitutive relationship simplifies to

$$\begin{bmatrix} \epsilon_x^0 \\ \kappa_x \end{bmatrix} = \begin{bmatrix} k_{11} & k_{12} \\ k_{12} & k_{22} \end{bmatrix} \begin{bmatrix} N_x \\ M_x \end{bmatrix}. \quad (\text{A.1a})$$

Under the cylindrical bending laminate condition (the plane strain condition), the deformation of the laminate is a function of its axial position x , with the terms, ϵ_x^0 , κ_y , and κ_{xy} equal to zero. Thus, the in-plane mid-plane strain and curvature can be determined as:

$$\begin{bmatrix} \epsilon_x^0 \\ \gamma_{xy}^0 \\ \kappa_x \end{bmatrix} = \begin{bmatrix} A_{11} & A_{16} & B_{11} \\ A_{16} & A_{66} & B_{16} \\ B_{11} & B_{16} & D_{11} \end{bmatrix}^{-1} \begin{bmatrix} N_x \\ N_{xy} \\ M_x \end{bmatrix}, \quad (\text{A.1b})$$

where A_{ij} , B_{ij} , and D_{ij} are elements in the stiffness (**ABD**) matrix of the laminate constitutive equation; N_x , N_{xy} , and M_x are unit-width in-plane forces and moments.

The in-plane shear force N_{xy} is equal to zero in this bending situation; hence, (A.1b) becomes

$$\begin{bmatrix} \epsilon_x^0 \\ \kappa_x \end{bmatrix} = \frac{\begin{bmatrix} A_{66}D_{11} - B_{16}^2 & A_{16}B_{16} - A_{66}B_{11} \\ A_{16}B_{16} - A_{66}B_{11} & A_{11}A_{66} - A_{16}^2 \end{bmatrix} \begin{bmatrix} N_x \\ M_x \end{bmatrix}}{A_{11}(A_{66}D_{11} - B_{16}^2) + 2A_{16}B_{11}B_{16} - D_{11}A_{16}^2 - A_{66}B_{11}^2}. \quad (\text{A.1c})$$

The corresponding k_{ij} term can be determined by comparing (A.1a) and (A.1b). The effective Young's modulus and bending stiffness are

$$E_{xx} = \frac{1}{t(A_{66}D_{11} - B_{16}^2)}(A_{11}(A_{66}D_{11} - B_{16}^2) + 2A_{16}B_{11}B_{16} - D_{11}A_{16}^2 - A_{66}B_{11}^2), \quad (\text{A.1d})$$

$$D_x = (EI)_{xx} = \frac{1}{(A_{11}A_{66} - A_{16}^2)}(D_{11}(A_{11}A_{66} - A_{16}^2) + 2A_{16}B_{11}B_{16} - A_{11}B_{16}^2 - A_{66}B_{11}^2), \quad (\text{A.1e})$$

where t is the laminate thickness. When the laminate is symmetrical and balanced, $B_{ij} = 0$ and $A_{16} = A_{26} = 0$. The effective parameters, E_{xx} and D_x , can be further simplified as:

$$E_{xx} = \frac{1}{tk_{11}} = \frac{A_{11}}{t}, \quad D_x = (EI)_{xx} = \frac{M_x}{\kappa_x} = D_{11}. \quad (\text{A.1f})$$

Integral constants for adhesive shear stresses (3c) and adhesive peel stresses (3e) in the special joint case. Let $Q = \sqrt[4]{b_1/4}$. Then

$$C_{0S} = \frac{1}{c} \left(-\frac{T}{2} + \frac{k_{11}T + \frac{1}{4}tk_{22}(M_0 - M_1)}{2k_{11} + \frac{1}{2}t^2k_{22}} \right), \quad (\text{A.2a})$$

$$C_{1S} = \frac{\frac{G_a}{\eta}(-k_{11}T + \frac{1}{4}tk_{22}(M_1 - M_0))}{\sqrt{-a_1} \sinh(c\sqrt{-a_1})}, \quad C_{2S} = \frac{\frac{G_a}{\eta} \frac{1}{4}tk_{22}(M_0 + M_1)}{\sqrt{-a_1} \cosh(c\sqrt{-a_1})};$$

$$C_{3S} = \frac{\frac{E_a}{2\eta}k_{22} \cosh c Q \cos c Q \left(\frac{V_0 + V_1}{Q^3} + \frac{M_0 - M_1}{Q^2} (\tanh c Q - \tan c Q) \right)}{\sinh 2c Q + \sin 2c Q},$$

$$C_{4S} = \frac{\frac{E_a}{2\eta}k_{22} \sinh c Q \cos c Q \left(\frac{V_0 - V_1}{Q^3} + \frac{M_0 + M_1}{Q^2} \left(\frac{1}{\tanh c Q} - \tan c Q \right) \right)}{\sin 2c Q - \sinh 2c Q}, \quad (\text{A.2b})$$

$$C_{5S} = \frac{\frac{E_a}{2\eta}k_{22} \cosh c Q \sin c Q \left(\frac{V_0 - V_1}{Q^3} + \frac{M_0 + M_1}{Q^2} \left(\tanh c Q + \frac{1}{\tan c Q} \right) \right)}{\sin 2c Q - \sinh 2c Q},$$

$$C_{6S} = \frac{\frac{E_a}{2\eta}k_{22} \sinh c Q \sin c Q \left(\frac{V_0 + V_1}{Q^3} + \frac{M_0 - M_1}{Q^2} \left(\frac{1}{\tanh c Q} + \frac{1}{\tan c Q} \right) \right)}{\sin 2c Q + \sinh 2c Q}.$$

Adhesive shear stress solution in the general joint case. The details on the derivation of the seven λ roots can be found from the [Li 2010]. They are

$$\lambda_0 = 0, \quad \lambda_{1,2} = \pm \sqrt{\gamma_1 - \frac{a_1}{3}}, \quad \lambda_{3,4} = \pm |\phi|^{\frac{1}{2}} \left(\cos \frac{\beta}{2} + i \sin \frac{\beta}{2} \right), \quad \lambda_{5,6} = \pm |\phi|^{\frac{1}{2}} \left(\cos \frac{\beta}{2} - i \sin \frac{\beta}{2} \right), \quad (\text{A.3a})$$

where

$$\gamma_1 = \sqrt[3]{-\frac{q}{2} + \sqrt{\left(\frac{q}{2}\right)^2 + \left(\frac{p}{3}\right)^3}} + \sqrt[3]{-\frac{q}{2} - \sqrt{\left(\frac{q}{2}\right)^2 + \left(\frac{p}{3}\right)^3}}, \quad p = b_1 - \frac{a_1^2}{3}, \quad q = \frac{2a_1^3}{27} + \frac{2a_1b_1}{3} - a_2b_2$$

$$|\phi| = \sqrt{\left(-\frac{\gamma_1}{2} - \frac{a_1}{3}\right)^2 + \frac{3}{4} \left(\sqrt[3]{-\frac{q}{2} + \sqrt{\left(\frac{q}{2}\right)^2 + \left(\frac{p}{3}\right)^3}} + \sqrt[3]{\frac{q}{2} + \sqrt{\left(\frac{q}{2}\right)^2 + \left(\frac{p}{3}\right)^3}} \right)^2}, \quad \beta = \min\{\beta_1, \beta_2\}.$$

The angles β_1 and β_2 are defined within the 0 to 2π range. The sum of the two angles is 2π . The angles are measured in radians and positive in the counterclockwise sense. For instance, if the angle β_1 is within the range 0 to $\pi/2$, the angles can be calculated to be

$$\beta_1 = \arctan \frac{\frac{\sqrt{3}}{2} \left(\sqrt[3]{-\frac{q}{2} + \sqrt{\left(\frac{q}{2}\right)^2 + \left(\frac{p}{3}\right)^3}} + \sqrt[3]{\frac{q}{2} + \sqrt{\left(\frac{q}{2}\right)^2 + \left(\frac{p}{3}\right)^3}} \right)}{-\frac{\gamma_1}{2} - \frac{a_1}{3}}, \quad \beta_2 = 2\pi - \beta_1. \quad (A.3b)$$

Expression of the adhesive shear stress in (5a). Details on the derivation of the following parameters, integral constants and functions can be found in [Li 2010]. Only the final expressions are provided in the following.

Submitting the shear stress from (5a) into the boundary conditions (5b), seven simultaneous equations written in terms of the seven constants C_0, \dots, C_6 are obtained:

$$\begin{aligned} C_0c + C_1C_{10} + C_3C_{30} + C_6C_{60} &= f_0, \\ -C_1C_{11} + C_2C_{21} - C_3C_{31} + C_4C_{41} + C_5C_{51} - C_6C_{61} &= f_1, \\ C_1C_{11} + C_2C_{21} + C_3C_{31} + C_4C_{41} + C_5C_{51} + C_6C_{61} &= f_2, \\ a_1C_0 + C_1C_{12} - C_2C_{22} + C_3C_{32} - C_4C_{42} - C_5C_{52} + C_6C_{62} &= f_3, \\ a_1C_0 + C_1C_{12} + C_2C_{22} + C_3C_{32} + C_4C_{42} + C_5C_{52} + C_6C_{62} &= f_4, \\ -C_1C_{13} + C_2C_{23} - C_3C_{33} + C_4C_{43} + C_5C_{53} - C_6C_{63} &= f_5, \\ C_1C_{13} + C_2C_{23} + C_3C_{33} + C_4C_{43} + C_5C_{53} + C_6C_{63} &= f_6. \end{aligned} \quad (A.3c)$$

The coefficients C_{ij} in (A.3c) are presented in [Li 2010]; they are omitted here for brevity. The final expressions for the seven constants are

$$\begin{aligned} C_6 &= \frac{\frac{f_3+f_4}{2} - f_0\frac{a_1}{c} + \frac{f_1-f_2}{2} \frac{C_{12}-C_{10}\frac{a_1}{c}}{C_{11}} - \left(\frac{f_6-f_5}{2} + \frac{f_1-f_2}{2} \frac{C_{13}}{C_{11}}\right) \frac{C_{32}-\frac{a_1}{c}C_{30}-\frac{C_{31}}{C_{11}}\left(C_{12}-C_{10}\frac{a_1}{c}\right)}{C_{33}-C_{31}C_{13}/C_{11}}}{C_{62}-\frac{a_1}{c}C_{60}-C_{61} \frac{C_{12}-C_{10}\frac{a_1}{c}}{C_{11}} - \left(C_{63}-C_{61} \frac{C_{13}}{C_{11}}\right) \frac{C_{32}-\frac{a_1}{c}C_{30}-\frac{C_{31}}{C_{11}}\left(C_{12}-C_{10}\frac{a_1}{c}\right)}{C_{33}-C_{31}C_{13}/C_{11}}}, \\ C_5 &= \frac{\frac{f_5+f_6}{2} - \frac{f_1+f_2}{2} \frac{C_{23}}{C_{21}} - \left(\frac{f_4-f_3}{2} - \frac{f_1+f_2}{2} \frac{C_{22}}{C_{21}}\right) \frac{C_{43}-C_{41}C_{23}/C_{21}}{C_{42}-C_{41}C_{22}/C_{21}}}{C_{53}-C_{51} \frac{C_{23}}{C_{21}} - \left(C_{52}-C_{51} \frac{C_{22}}{C_{21}}\right) \frac{C_{43}-C_{41}C_{23}/C_{21}}{C_{42}-C_{41}C_{22}/C_{21}}}, \\ C_4 &= \frac{1}{C_{42}-C_{41}C_{22}/C_{21}} \left(\frac{f_4-f_3}{2} - \frac{f_1+f_2}{2} \frac{C_{22}}{C_{21}} - C_5 \left(C_{52} - C_{51} \frac{C_{22}}{C_{21}} \right) \right), \\ C_3 &= \frac{1}{C_{33}-C_{31}C_{13}/C_{11}} \left(\frac{f_6-f_5}{2} + \frac{f_1-f_2}{2} \frac{C_{13}}{C_{11}} - C_6 \left(C_{63} - C_{61} \frac{C_{13}}{C_{11}} \right) \right), \end{aligned}$$

$$\begin{aligned} C_2 &= \frac{1}{C_{21}} \left(\frac{f_1 + f_2}{2} - C_{41}C_4 - C_{51}C_5 \right), \\ C_1 &= -\frac{1}{C_{11}} \left(\frac{f_1 - f_2}{2} + C_{31}C_3 + C_{61}C_6 \right), \\ C_0 &= \frac{1}{c} (f_0 - C_{10}C_1 - C_{30}C_3 - C_{60}C_6), \end{aligned}$$

where

$$\begin{aligned} f_0 &= -T/2, \\ f_1 &= \frac{G_a}{\eta} \left((k_{11,\text{adh}} + \frac{1}{2}t_1k_{12,\text{adh}})T + (k_{12,\text{adh}} + \frac{1}{2}t_1k_{22,\text{adh}})M_0 \right), \\ f_2 &= \frac{G_a}{\eta} \left((-k_{11,\text{doub}} + \frac{1}{2}t_2k_{12,\text{doub}})T + (-k_{12,\text{doub}} + \frac{1}{2}t_2k_{22,\text{doub}})M_1 \right), \\ f_3 &= \frac{G_a}{\eta} (k_{12,\text{adh}} + \frac{1}{2}t_1k_{22,\text{adh}})V_0, \quad f_4 = \frac{G_a}{\eta} (-k_{12,\text{doub}} + \frac{1}{2}t_2k_{22,\text{doub}})V_1, \\ f_5 &= -a_2 \frac{E_a}{\eta} (k_{12,\text{adh}}T + k_{22,\text{adh}}M_0), \quad f_6 = a_2 \frac{E_a}{\eta} (k_{12,\text{doub}}T + k_{22,\text{doub}}M_1). \end{aligned}$$

Expression of the adhesive peel stress using the first strategy. Let $Q = \sqrt[4]{b_1/4}$. The four constants in (6a) and (6d) are

$$\begin{aligned} C_{1H} &= \frac{\frac{E_a}{2\eta} \cosh c Q \cos c Q \left(\frac{k_{22,\text{adh}}V_0 + k_{22,\text{doub}}V_1}{Q^3} + \frac{k_{12}^-T + k_{22,\text{adh}}M_0 - k_{22,\text{doub}}M_1}{Q^2} (\tanh c Q - \tan c Q) \right)}{\sinh 2c Q + \sin 2c Q} \\ &\quad - \frac{\cosh c Q \cos c Q}{2(\sinh 2c Q + \sin 2c Q)} \frac{b_2(\tau_a(-c) - \tau_a(c))}{Q^3} + H_1, \\ C_{2H} &= \frac{\frac{E_a}{2\eta} \sinh c Q \cos c Q \left(\frac{k_{22,\text{adh}}V_0 - k_{22,\text{doub}}V_1}{Q^3} + \frac{k_{12}^+T + k_{22,\text{adh}}M_0 + k_{22,\text{doub}}M_1}{Q^2} \left(\frac{1}{\tanh c Q} - \tan c Q \right) \right)}{\sin 2c Q - \sinh 2c Q} \\ &\quad + \frac{\sinh c Q \cos c Q}{2(\sin 2c Q - \sinh 2c Q)} \frac{b_2(\tau_a(-c) + \tau_a(c))}{Q^3} + H_2, \\ C_{3H} &= \frac{\frac{E_a}{2\eta} \cosh c Q \sin c Q \left(\frac{k_{22,\text{adh}}V_0 - k_{22,\text{doub}}V_1}{Q^3} + \frac{k_{12}^+T + k_{22,\text{adh}}M_0 + k_{22,\text{doub}}M_1}{Q^2} \left(\tanh c Q + \frac{1}{\tan c Q} \right) \right)}{\sin 2c Q - \sinh 2c Q} \\ &\quad + \frac{\cosh c Q \sin c Q}{2(\sinh 2c Q - \sin 2c Q)} \frac{b_2(\tau_a(-c) + \tau_a(c))}{Q^3} + H_3, \\ C_{4H} &= \frac{\frac{E_a}{2\eta} \sinh c Q \sin c Q \left(\frac{k_{22,\text{adh}}V_0 + k_{22,\text{doub}}V_1}{Q^3} + \frac{k_{12}^-T + k_{22,\text{adh}}M_0 - k_{22,\text{doub}}M_1}{Q^2} \left(\frac{1}{\tanh c Q} + \frac{1}{\tan c Q} \right) \right)}{\sin 2c Q + \sinh 2c Q} \\ &\quad - \frac{\sinh c Q \sin c Q}{(\sin 2c Q + \sinh 2c Q)} \frac{b_2(\tau_a(-c) - \tau_a(c))}{Q^3} + H_4, \end{aligned} \tag{A.4}$$

where

$$k_{12}^+ = k_{12,\text{adh}} + k_{12,\text{doub}}, \quad k_{12}^- = k_{12,\text{adh}} - k_{12,\text{doub}},$$

$$H_1 = -\frac{1}{2}(G_{1p}(-c) + G_{1p}(c)) + \frac{\cosh^2 c Q(G_{2p}(-c) - G_{2p}(c))}{\sinh 2c Q + \sin 2c Q} - \frac{\cos^2 c Q(G_{3p}(-c) - G_{3p}(c))}{\sinh 2c Q + \sin 2c Q},$$

$$H_2 = \frac{\sinh^2 c Q(G_{1p}(-c) - G_{1p}(c))}{\sinh 2c Q - \sin 2c Q} - \frac{1}{2}(G_{2p}(-c) + G_{2p}(c)) + \frac{\cos^2 c Q(G_{4p}(-c) - G_{4p}(c))}{\sinh 2c Q - \sin 2c Q},$$

$$H_3 = \frac{\sin^2 c Q(G_{1p}(-c) - G_{1p}(c))}{\sinh 2c Q - \sin 2c Q} - \frac{1}{2}(G_{3p}(-c) + G_{3p}(c)) + \frac{\cosh^2 c Q(G_{4p}(-c) - G_{4p}(c))}{\sinh 2c Q - \sin 2c Q},$$

$$H_4 = -\frac{\sin^2 c Q(G_{2p}(-c) - G_{2p}(c))}{\sinh 2c Q + \sin 2c Q} + \frac{\sinh^2 c Q(G_{3p}(-c) - G_{3p}(c))}{\sinh 2c Q + \sin 2c Q} - \frac{1}{2}(G_{4p}(-c) + G_{4p}(c)).$$

The six integral constants in the adhesive peel stress expression using the second strategy. Submitting the peel stress from (7c) into the boundary conditions Equation (7d), six simultaneous equations written in terms of the six constants C_{p1}, \dots, C_{p6} can be obtained:

$$\begin{aligned} C_{p1}I_{11} + C_{p3}I_{31} + C_{p6}I_{61} &= g_1, \\ C_{p2}I_{22} + C_{p4}I_{42} + C_{p5}I_{52} &= g_2, \\ C_{p1}I_{13} - C_{p2}I_{23} + C_{p3}I_{33} - C_{p4}I_{43} - C_{p5}I_{53} + C_{p6}I_{63} &= g_3, \\ C_{p1}I_{13} + C_{p2}I_{23} + C_{p3}I_{33} + C_{p4}I_{43} + C_{p5}I_{53} + C_{p6}I_{63} &= g_4, \\ -C_{p1}I_{14} + C_{p2}I_{24} - C_{p3}I_{34} + C_{p4}I_{44} + C_{p5}I_{54} - C_{p6}I_{64} &= g_5, \\ C_{p1}I_{14} + C_{p2}I_{24} + C_{p3}I_{34} + C_{p4}I_{44} + C_{p5}I_{54} + C_{p6}I_{64} &= g_6. \end{aligned} \tag{A.5a}$$

The final expressions for the six constants are

$$\begin{aligned} C_{p6} &= \frac{\frac{g_5 - g_6}{2} + g_1 \frac{I_{14}}{I_{11}} + \left(\frac{g_3 + g_4}{2} - g_1 \frac{I_{13}}{I_{11}}\right) \frac{I_{11}I_{34} - I_{31}I_{14}}{I_{11}I_{33} - I_{31}I_{13}}}{-I_{64} + I_{61} \frac{I_{14}}{I_{11}} + \left(I_{63} - I_{61} \frac{I_{13}}{I_{11}}\right) \frac{I_{11}I_{34} - I_{31}I_{14}}{I_{11}I_{33} - I_{31}I_{13}}}, \\ C_{p5} &= \frac{\frac{g_5 + g_6}{2} - g_2 \frac{I_{24}}{I_{22}} - \left(\frac{g_4 - g_3}{2} - g_2 \frac{I_{23}}{I_{22}}\right) \frac{I_{22}I_{44} - I_{42}I_{24}}{I_{22}I_{43} - I_{42}I_{23}}}{I_{54} - I_{52} \frac{I_{24}}{I_{22}} - \left(I_{53} - I_{52} \frac{I_{23}}{I_{22}}\right) \frac{I_{22}I_{44} - I_{42}I_{24}}{I_{22}I_{43} - I_{42}I_{23}}}, \\ C_{p4} &= \frac{\frac{g_4 - g_3}{2} - g_2 \frac{I_{23}}{I_{22}} - C_{p5} \left(I_{53} - I_{52} \frac{I_{23}}{I_{22}}\right)}{I_{43} - I_{42} \frac{I_{23}}{I_{22}}}, \end{aligned}$$

$$C_{p3} = \frac{\frac{g_3 + g_4}{2} - g_1 \frac{I_{13}}{I_{11}} - C_{p6}(I_{63} - I_{61} \frac{I_{13}}{I_{11}})}{I_{33} - I_{31} \frac{I_{13}}{I_{11}}},$$

$$C_{p2} = \frac{1}{I_{22}}(g_2 - C_{p4}I_{42} - C_{p5}I_{52}), \quad C_{p1} = \frac{1}{I_{11}}(g_1 - C_{p3}I_{31} - C_{p6}I_{61}).$$

where

$$g_1 = \frac{V_0}{2}, \quad g_2 = -\frac{cV_0 + M_0}{2}, \quad g_3 = \frac{E_a}{\eta}(k_{12,\text{adh}}T + k_{22,\text{adh}}M_0), \quad g_4 = -\frac{E_a}{\eta}(k_{12,\text{doub}}T + k_{22,\text{doub}}M_1),$$

$$g_5 = \frac{E_a}{\eta}k_{22,\text{adh}}V_0 - b_2\tau_a|_{x=-c}, \quad g_6 = -\frac{E_a}{\eta}k_{22,\text{doub}}V_1 - b_2\tau_a|_{x=c},$$

$$I_{11} = C_{10} = \frac{\sinh c\sqrt{\gamma_1 - a_1/3}}{\sqrt{\gamma_1 - a_1/3}},$$

$$I_{31} = C_{30} = \sin \frac{\beta}{2} |\phi|^{-\frac{1}{2}} (\cosh(c|\phi|^{\frac{1}{2}} \cos \frac{\beta}{2}) \sin(c|\phi|^{\frac{1}{2}} \sin \frac{\beta}{2}) + \cot \frac{\beta}{2} \sinh(c|\phi|^{\frac{1}{2}} \cos \frac{\beta}{2}) \cos(c|\phi|^{\frac{1}{2}} \sin \frac{\beta}{2})),$$

$$I_{61} = C_{60} = \sin \frac{\beta}{2} |\phi|^{-\frac{1}{2}} (-\sinh(c|\phi|^{\frac{1}{2}} \cos \frac{\beta}{2}) \cos(c|\phi|^{\frac{1}{2}} \sin \frac{\beta}{2}) + \cot \frac{\beta}{2} \cosh(c|\phi|^{\frac{1}{2}} \cos \frac{\beta}{2}) \sin(c|\phi|^{\frac{1}{2}} \sin \frac{\beta}{2})),$$

$$I_{22} = \frac{c}{\sqrt{\gamma_1 - a_1/3}} \cosh c\sqrt{\gamma_1 - a_1/3} - \frac{1}{\gamma_1 - a_1/3} \sinh c\sqrt{\gamma_1 - a_1/3},$$

$$I_{42} = c \sin \frac{\beta}{2} |\phi|^{-\frac{1}{2}} \sinh(c|\phi|^{\frac{1}{2}} \cos \frac{\beta}{2}) \sin(c|\phi|^{\frac{1}{2}} \sin \frac{\beta}{2}) + c \cos \frac{\beta}{2} |\phi|^{-\frac{1}{2}} \cosh(c|\phi|^{\frac{1}{2}} \cos \frac{\beta}{2}) \cos(c|\phi|^{\frac{1}{2}} \sin \frac{\beta}{2}) \\ - \sin \frac{\beta}{2} |\phi|^{-1} \cosh(c|\phi|^{\frac{1}{2}} \cos \frac{\beta}{2}) \sin(c|\phi|^{\frac{1}{2}} \sin \frac{\beta}{2}) - \cos \frac{\beta}{2} |\phi|^{-1} \sinh(c|\phi|^{\frac{1}{2}} \cos \frac{\beta}{2}) \cos(c|\phi|^{\frac{1}{2}} \sin \frac{\beta}{2}),$$

$$I_{52} = c \cos \frac{\beta}{2} |\phi|^{-\frac{1}{2}} \sinh(c|\phi|^{\frac{1}{2}} \cos \frac{\beta}{2}) \sin(c|\phi|^{\frac{1}{2}} \sin \frac{\beta}{2}) - c \sin \frac{\beta}{2} |\phi|^{-\frac{1}{2}} \cosh(c|\phi|^{\frac{1}{2}} \cos \frac{\beta}{2}) \cos(c|\phi|^{\frac{1}{2}} \sin \frac{\beta}{2}) \\ + \cos \frac{\beta}{2} |\phi|^{-1} \cosh(c|\phi|^{\frac{1}{2}} \cos \frac{\beta}{2}) \sin(c|\phi|^{\frac{1}{2}} \sin \frac{\beta}{2}) + \sin \frac{\beta}{2} |\phi|^{-1} \sinh(c|\phi|^{\frac{1}{2}} \cos \frac{\beta}{2}) \cos(c|\phi|^{\frac{1}{2}} \sin \frac{\beta}{2}),$$

$$I_{13} = (\gamma_1 - a_1/3) \cosh c\sqrt{\gamma_1 - a_1/3}, \quad I_{23} = (\gamma_1 - a_1/3) \sinh c\sqrt{\gamma_1 - a_1/3},$$

$$I_{33} = |\phi| \left(\cos \beta \cosh(c|\phi|^{\frac{1}{2}} \cos \frac{\beta}{2}) \cos(c|\phi|^{\frac{1}{2}} \sin \frac{\beta}{2}) - \sin \beta \sinh(c|\phi|^{\frac{1}{2}} \cos \frac{\beta}{2}) \sin(c|\phi|^{\frac{1}{2}} \sin \frac{\beta}{2}) \right),$$

$$I_{43} = |\phi| \left(\cos \beta \sinh(c|\phi|^{\frac{1}{2}} \cos \frac{\beta}{2}) \cos(c|\phi|^{\frac{1}{2}} \sin \frac{\beta}{2}) - \sin \beta \cosh(c|\phi|^{\frac{1}{2}} \cos \frac{\beta}{2}) \sin(c|\phi|^{\frac{1}{2}} \sin \frac{\beta}{2}) \right),$$

$$I_{53} = |\phi| \left(\cos \beta \cosh(c|\phi|^{\frac{1}{2}} \cos \frac{\beta}{2}) \sin(c|\phi|^{\frac{1}{2}} \sin \frac{\beta}{2}) + \sin \beta \sinh(c|\phi|^{\frac{1}{2}} \cos \frac{\beta}{2}) \cos(c|\phi|^{\frac{1}{2}} \sin \frac{\beta}{2}) \right),$$

$$I_{63} = |\phi| \left(\cos \beta \sinh(c|\phi|^{\frac{1}{2}} \cos \frac{\beta}{2}) \sin(c|\phi|^{\frac{1}{2}} \sin \frac{\beta}{2}) + \sin \beta \cosh(c|\phi|^{\frac{1}{2}} \cos \frac{\beta}{2}) \cos(c|\phi|^{\frac{1}{2}} \sin \frac{\beta}{2}) \right),$$

$$I_{14} = (\gamma_1 - a_1/3)^{\frac{3}{2}} \sinh c\sqrt{\gamma_1 - a_1/3}, \quad I_{24} = (\gamma_1 - a_1/3)^{\frac{3}{2}} \cosh c\sqrt{\gamma_1 - a_1/3},$$

$$I_{34} = |\phi|^{\frac{3}{2}} \left(\cos \frac{3\beta}{2} \sinh(c|\phi|^{\frac{1}{2}} \cos \frac{\beta}{2}) \cos(c|\phi|^{\frac{1}{2}} \sin \frac{\beta}{2}) - \sin \frac{3\beta}{2} \cosh(c|\phi|^{\frac{1}{2}} \cos \frac{\beta}{2}) \sin(c|\phi|^{\frac{1}{2}} \sin \frac{\beta}{2}) \right),$$

$$I_{44} = |\phi|^{\frac{3}{2}} \left(\cos \frac{3\beta}{2} \cosh(c|\phi|^{\frac{1}{2}} \cos \frac{\beta}{2}) \cos(c|\phi|^{\frac{1}{2}} \sin \frac{\beta}{2}) - \sin \frac{3\beta}{2} \sinh(c|\phi|^{\frac{1}{2}} \cos \frac{\beta}{2}) \sin(c|\phi|^{\frac{1}{2}} \sin \frac{\beta}{2}) \right),$$

$$I_{54} = |\phi|^{\frac{3}{2}} \left(\cos \frac{3\beta}{2} \sinh(c|\phi|^{\frac{1}{2}} \cos \frac{\beta}{2}) \sin(c|\phi|^{\frac{1}{2}} \sin \frac{\beta}{2}) + \sin \frac{3\beta}{2} \cosh(c|\phi|^{\frac{1}{2}} \cos \frac{\beta}{2}) \cos(c|\phi|^{\frac{1}{2}} \sin \frac{\beta}{2}) \right),$$

$$I_{64} = |\phi|^{\frac{3}{2}} \left(\cos \frac{3\beta}{2} \cosh(c|\phi|^{\frac{1}{2}} \cos \frac{\beta}{2}) \sin(c|\phi|^{\frac{1}{2}} \sin \frac{\beta}{2}) + \sin \frac{3\beta}{2} \sinh(c|\phi|^{\frac{1}{2}} \cos \frac{\beta}{2}) \cos(c|\phi|^{\frac{1}{2}} \sin \frac{\beta}{2}) \right).$$

List of symbols

Only important symbols are listed. Unlisted symbols are explained in the text.

$2c$	bonded overlap length on one adherend side
L	the length of the outer unbonded adherend
$2L_0$	the length of the inner unbonded doubler
t_1	adherend laminate thickness
t_2	doubler laminate thickness
M_0, M_1	unit-width bending moments at the outer and inner bonded overlap edges
k_{ij}	compliance terms ($i, j = 1$ and 2) defined in (A.1a)
T	joint remote unit-width tensile force
V_0, V_1	unit-width shear forces at the outer and inner bonded overlap edges
η	adhesive layer thickness
σ_a, τ_a	adhesive peel and shear stresses
E_a, G_a	adhesive Young's and shear moduli
a_1, a_2, b_1, b_2	joint parameters defined in (2b), (2c), (2d), and (2e)

References

- [Bigwood and Crocombe 1989] D. A. Bigwood and A. D. Crocombe, "Elastic analysis and engineering design formulae for bonded joints", *Int. J. Adhes. Adhes.* **9**:4 (1989), 229–242.
- [Chen and Cheng 1983] D. Chen and S. Cheng, "An analysis of adhesive-bonded single-lap joints", *J. Appl. Mech. (ASME)* **50**:1 (1983), 109–115.
- [Cheng et al. 1991] S. Cheng, D. Chen, and Y. Shi, "Analysis of adhesive-bonded joints with nonidentical adherends", *J. Eng. Mech. (ASCE)* **117**:3 (1991), 605–623.
- [Delale et al. 1981] F. Delale, F. Erdogan, and M. N. Aydinoglu, "Stresses in adhesively bonded joints: a closed-form solution", *J. Compos. Mater.* **15**:3 (1981), 249–271.
- [Derrick and Grossman 1987] W. R. Derrick and S. I. Grossman, *A first course in differential equations with applications*, 3rd ed., West Publishing, St. Paul, MN, 1987.
- [Goland and Reissner 1944] M. Goland and E. Reissner, "The stresses in cemented joints", *J. Appl. Mech. (ASME)* **11** (1944), A17–A27.
- [Hart-Smith 1973] L. J. Hart-Smith, "Adhesive-bonded single lap joints", Contractor Report 112236, Douglas Aircraft Company, Long Beach, CA, 1973, available at <http://tinyurl.com/NASA-CR-112236>.
- [Hart-Smith 1985] L. J. Hart-Smith, "Designing to minimize peel stresses in adhesive-bonded joints", pp. 238–266 in *Delamination and debonding of materials* (Pittsburgh, PA, 1983), edited by W. S. Johnson, ASTM Special Technical Publication **876**, American Society for Testing and Materials, Philadelphia, 1985.
- [Hu 1995] G. Hu, "Mixed mode fracture analysis of adhesive lap joints", *Compos. Eng.* **5**:8 (1995), 1043–1050.
- [Kelly 2006] G. Kelly, "Quasi-static strength and fatigue life of hybrid (bonded/bolted) composite single-lap joints", *Compos. Struct.* **72**:1 (2006), 119–129.
- [Kreyszig 1993] E. Kreyszig, *Advanced engineering mathematics*, 7th ed., Wiley, New York, 1993.
- [Li 2008] G. Li, "Exploration of closed-form solutions for adhesive stresses in bonded single-strap butt joints", Laboratory Technical Report LTR-SMPL-2008-0174, NRC Institute for Aerospace Research, National Research Council Canada, Ottawa, ON, 2008.
- [Li 2010] G. Li, "Elastic analysis of closed-form solutions for adhesive stresses in bonded single-strap butt joints", *J. Mech. Mater. Struct.* **5**:3 (2010), 409–426.

- [Li and Lee-Sullivan 2006a] G. Li and P. Lee-Sullivan, “Re-visiting the beam models for adhesively bonded single-lap joints, I: Comparison of bending moment predictions”, *Can. Aeronaut. Space. J.* **52**:4 (2006), 149–171.
- [Li and Lee-Sullivan 2006b] G. Li and P. Lee-Sullivan, “Re-visiting the beam models for adhesively bonded single-lap joints, II: Comparison of the adhesive stress predictions”, *Can. Aeronaut. Space. J.* **52**:4 (2006), 173–180.
- [Li et al. 1999] G. Li, P. Lee-Sullivan, and R. W. Thring, “Nonlinear finite element analysis of stress and strain distributions across the adhesive thickness in composite single-lap joints”, *Compos. Struct.* **46**:4 (1999), 395–403.
- [Li et al. 2011] G. Li, A. Johnston, M. Yanishevsky, and N. C. Bellinger, “Elastic deformation analysis of adhesively bonded composite butt joints in tension”, *J. Aircraft* **48**:2 (2011), 578–590.
- [Li et al. 2012] G. Li, J. H. Chen, M. Yanishevsky, and N. C. Bellinger, “Static strength of a composite butt joint configuration with different attachments”, *Compos. Struct.* **94**:5 (2012), 1736–1744.
- [Oplinger 1994] D. W. Oplinger, “Effects of adherend deflections in single lap joints”, *Int. J. Solids Struct.* **31**:18 (1994), 2565–2587.
- [Volkersen 1938] O. Volkersen, “Die Nietkraftverteilung in zugbeanspruchten Nietverbindungen mit konstanten Laschenquerschnitten”, *Luftfahrtforsch.* **15** (1938), 41–47.

Received 1 Sep 2011. Revised 24 Nov 2011. Accepted 13 Jan 2012.

GANG LI: Gang.Li@nrc-cnrc.gc.ca

Structures Group, Aerospace Portfolio, National Research Council Canada, M-3, 1200 Montreal Road, Ottawa ON K1A 0R6, Canada

JOURNAL OF MECHANICS OF MATERIALS AND STRUCTURES

jomms.net

Founded by Charles R. Steele and Marie-Louise Steele

EDITORS

CHARLES R. STEELE Stanford University, USA
DAVIDE BIGONI University of Trento, Italy
IWONA JASIUK University of Illinois at Urbana-Champaign, USA
YASUhide SHINDO Tohoku University, Japan

EDITORIAL BOARD

H. D. BUI École Polytechnique, France
J. P. CARTER University of Sydney, Australia
R. M. CHRISTENSEN Stanford University, USA
G. M. L. GLADWELL University of Waterloo, Canada
D. H. HODGES Georgia Institute of Technology, USA
J. HUTCHINSON Harvard University, USA
C. HWU National Cheng Kung University, Taiwan
B. L. KARIHALOO University of Wales, UK
Y. Y. KIM Seoul National University, Republic of Korea
Z. MROZ Academy of Science, Poland
D. PAMPLONA Universidade Católica do Rio de Janeiro, Brazil
M. B. RUBIN Technion, Haifa, Israel
A. N. SHUPIKOV Ukrainian Academy of Sciences, Ukraine
T. TARNAI University Budapest, Hungary
F. Y. M. WAN University of California, Irvine, USA
P. WRIGGERS Universität Hannover, Germany
W. YANG Tsinghua University, China
F. ZIEGLER Technische Universität Wien, Austria

PRODUCTION contact@msp.org

SILVIO LEVY Scientific Editor

Cover design: Alex Scorpan

Cover photo: Mando Gomez, www.mandolux.com

See <http://jomms.net> for submission guidelines.

JoMMS (ISSN 1559-3959) is published in 10 issues a year. The subscription price for 2012 is US \$555/year for the electronic version, and \$735/year (+\$60 shipping outside the US) for print and electronic. Subscriptions, requests for back issues, and changes of address should be sent to Mathematical Sciences Publishers, Department of Mathematics, University of California, Berkeley, CA 94720-3840.

JoMMS peer-review and production is managed by EditFLOW[®] from Mathematical Sciences Publishers.

PUBLISHED BY
 **mathematical sciences publishers**
<http://msp.org/>

A NON-PROFIT CORPORATION

Typeset in L^AT_EX

Copyright ©2012 by Mathematical Sciences Publishers

Journal of Mechanics of Materials and Structures

Volume 7, No. 4

April 2012

- Analytical study of plastic deformation of clamped circular plates subjected to impulsive loading** **HASHEM BABAEI and ABOLFAZL DARVIZEH** **309**
- Theoretical solutions of adhesive stresses in bonded composite butt joints** **GANG LI** **323**
- Micromechanical study of dispersion and damping characteristics of granular materials** **NIELS P. KRUYT** **347**
- Buckling instabilities of elastically connected Timoshenko beams on an elastic layer subjected to axial forces** **VLADIMIR STOJANOVIĆ, PREDRAG KOZIĆ and GORAN JANEVSKI** **363**
- The effective thickness of laminated glass plates** **LAURA GALUPPI and GIANNI ROYER-CARFAGNI** **375**
- Elastic solution in a functionally graded coating subjected to a concentrated force** **ROBERTA SBURLATI** **401**



1559-3959(2012)7:4;1-A